ZU-TH 16/16
MITP/16-038
NSF-KITP-16-047
DESY 16-075

arXiv:1605.02716v1 [hep-ph] 9 May 2016

W^+W^- production at the LHC: fiducial cross sections and distributions in NNLO QCD

Massimiliano Grazzini[(a)], **Stefan Kallweit**[(b,c)], **Stefano Pozzorini**[(a,c)], **Dirk Rathlev**[(d)] and **Marius Wiesemann**[(a)]

[(a)] Physik-Institut, Universität Zürich, CH-8057 Zürich, Switzerland

[(b)] PRISMA Cluster of Excellence, Institute of Physics, Johannes Gutenberg University, D-55099 Mainz, Germany

[(c)] Kavli Institute for Theoretical Physics, University of California, Santa Barbara, CA 93106, USA

[(d)] Theory Group, Deutsches Elektronen-Synchrotron (DESY), D-22607 Hamburg, Germany

Abstract

We consider QCD radiative corrections to W^+W^- production at the LHC and present the first fully differential predictions for this process at next-to-next-to-leading order (NNLO) in perturbation theory. Our computation consistently includes the leptonic decays of the W bosons, taking into account spin correlations, off-shell effects and non-resonant contributions. Detailed predictions are presented for the different-flavour channel $pp \to \mu^+ e^- \nu_\mu \bar{\nu}_e + X$ at $\sqrt{s} = 8$ and 13 TeV. In particular, we discuss fiducial cross sections and distributions in the presence of standard selection cuts used in experimental W^+W^- and $H \to W^+W^-$ analyses at the LHC. The inclusive W^+W^- cross section receives large NNLO corrections, and, due to the presence of a jet veto, typical fiducial cuts have a sizeable influence on the behaviour of the perturbative expansion. The availability of differential NNLO predictions, both for inclusive and fiducial observables, will play an important role in the rich physics programme that is based on precision studies of W^+W^- signatures at the LHC.

May 2016

1 Introduction

The production of W-boson pairs is one of the most important electroweak (EW) processes at hadron colliders. Experimental studies of W^+W^- production play a central role in precision tests of the gauge symmetry structure of EW interactions and of the mechanism of EW symmetry breaking. The W^+W^- cross section has been measured at the Tevatron [1,2] and at the LHC, both at 7 TeV [3,4] and 8 TeV [5–8]. The dynamics of W-pair production is of great interest, not only in the context of precision tests of the Standard Model, but also in searches of physics beyond the Standard Model (BSM). Any small anomaly in the production rate or in the shape of distributions could be a signal of new physics. In particular, due to the high sensitivity to modifications of the Standard Model trilinear gauge couplings, W^+W^- measurements are a powerful tool for indirect BSM searches via anomalous couplings [3,4,6,8,9]. Thanks to the increasing reach in transverse momentum, Run 2 of the LHC will considerably tighten the present bounds on anomalous couplings. Final states with W-boson pairs are widely studied also in the context of direct BSM searches [10].

In Higgs-boson studies [11–16], W^+W^- production plays an important role as irreducible background in the $H \to W^+W^-$ channel. Such measurements are mostly based on final states with two leptons and two neutrinos, which provide a clean experimental signature, but do not allow for a full reconstruction of the $H \to W^+W^-$ resonance. As a consequence, it is not possible to extract the irreducible W^+W^- background from data with a simple side-band approach. Thus, the availability of precise theory predictions for the W^+W^- background is essential for the sensitivity to $H \to W^+W^-$ and to any BSM particle that decays into W-boson pairs.In the context of Higgs studies, the off-shell treatment of W-boson decays is of great relevance, both for the description of the $H \to W^+W^-$ signal region below the W^+W^- threshold, and for indirect determinations of the Higgs-boson width through signal–background interference effects at high invariant masses [17–19].

The accurate description of the jet activity is another critical aspect of Higgs measurements, and of W^+W^- measurements in general. Such analyses typically rely on a rather strict jet veto, which suppresses the severe signal contamination due to the $t\bar{t}$ background, but induces potentially large logarithms that challenge the reliability of fixed-order predictions in perturbation theory. All these requirements, combined with the ever increasing accuracy of experimental measurements, call for continuous improvements in the theoretical description of W^+W^- production.

Next-to-leading order (NLO) QCD predictions for W^+W^- production at hadron colliders have been available for a long time, both for the case of stable W-bosons [20,21] and with spin-correlated decays of vector bosons into leptons [22–25]. Recently, also the NLO EW corrections have been computed [26–28]. Their impact on inclusive cross sections hardly exceeds a few percent, but can be strongly enhanced up to several tens of percent at transverse momenta of about 1 TeV.

Given the sizeable impact of $\mathcal{O}(\alpha_S)$ corrections, the calculation of higher-order QCD effects is indispensable in order to reach high precision. The simplest ingredient of $pp \to W^+W^- + X$ at $\mathcal{O}(\alpha_S^2)$ is given by the loop-induced gluon-fusion contribution. Due to the strong enhancement of the gluon luminosity, the gg channel was generally regarded as the dominant source of NNLO QCD corrections to $pp \to W^+W^- + X$ in the literature. Predictions for $gg \to W^+W^-$ at LO have been widely studied [25, 29–32], and squared quark-loop contributions at LO are known also for $gg \to W^+W^-g$ [33, 34]. Two-loop helicity amplitudes for $gg \to VV'$ became available in Refs. [35, 36], and have been used to compute the NLO QCD corrections to $gg \to W^+W^-$ [37],

including all partonic processes with external gluons, while the ones with external quarks are still unknown to date. Calculations at NLO QCD for W^+W^- production in association with one [38–41] and two [42, 43] jets are also important ingredients of inclusive W^+W^- production at NNLO QCD and beyond. The merging of NLO QCD predictions for $pp \to W^+W^- + 0, 1\,\text{jets}$* has been presented in Ref. [45]. This merged calculation also consistently includes squared quark-loop contributions to $pp \to W^+W^- + 0, 1\,\text{jets}$ in all gluon- and quark-induced channels.

First NNLO QCD predictions for the inclusive W^+W^- cross section became available in Ref. [46]. This calculation was based on two-loop scattering amplitudes for on-shell W^+W^- production, while two-loop helicity amplitudes are now available for all vector-boson pair production processes, including off-shell leptonic decays [47, 48]. In the energy range from 7 to 14 TeV, NNLO corrections shift the NLO predictions for the total cross section by about 9% to 12% [46], which is around three times as large as the $gg \to W^+W^-$ contribution alone. Thus, contrary to what was widely expected, gluon–gluon fusion is not the dominant source of radiative corrections beyond NLO. Moreover, the relatively large size of NNLO effects turned out to alleviate the tension that was observed between earlier experimental measurements [5, 7] and NLO QCD predictions supplemented with the loop-induced gluon fusion contribution [25]. In fact, NNLO QCD predictions are in good agreement with the latest measurements of the W^+W^- cross section [6, 8].

Besides perturbative calculations for the inclusive cross section, the modelling of the jet-veto efficiency is another theoretical ingredient that plays a critical role in the comparison of data with Standard Model predictions. In particular, it was pointed out that a possible underestimate of the jet-veto efficiency through the Powheg Monte Carlo [49], which is used to extrapolate the measured cross section from the fiducial region to the full phase space, would lead to an artificial excess in the total cross section [50]. The relatively large size of higher-order effects and the large intrinsic uncertainties of NLO+PS Monte Carlo simulations call for improved theoretical predictions for the jet-veto efficiency. The resummation of logarithms of the jet-veto scale at next-to-next-to-leading logarithmic (NNLL) accuracy was presented in Refs. [51, 52]. Being matched to the $pp \to W^+W^- + X$ cross sections at NLO, these predictions cannot describe the vetoing of hard jets beyond LO accuracy. In order to reach higher theoretical accuracy, NNLL resummation needs to be matched to differential NNLO calculations. Such NNLL+NNLO predictions have been presented in Ref. [53] for the distribution in the transverse momentum of the W^+W^- system, and could be used to obtain accurate predictions for the jet-veto efficiency through a reweighting of Monte Carlo samples.

In this paper we present, for the first time, fully differential predictions for W^+W^- production with leptonic decays at NNLO. More precisely, the full process that leads to a final state with two leptons and two neutrinos is considered, including all relevant off-shell and interference effects in the complex-mass scheme [54]. The calculation is carried out with Matrix [55], a new tool that is based on the Munich Monte Carlo program [56] interfaced with the OpenLoops generator of one-loop scattering amplitudes [57, 58], and includes an automated implementation of the q_T-subtraction [59] and -resummation [60] formalisms. This widely automated framework has already been used, in combination with the two-loop scattering amplitudes of Refs. [48, 61], for the calculations of $Z\gamma$ [62, 63], ZZ [64, 65], W^+W^- [46], $W^\pm\gamma$ [63] and $W^\pm Z$ [66] production at NNLO QCD as well as in the resummed computations of the ZZ and W^+W^- transverse-momentum spectra [53] at NNLL+NNLO. The present calculation relies on the two-loop amplitudes of Ref. [48].

*See also [44] for a combination of fixed-order NLO predictions for W^+W^-+0,1 jet production.

Their implementation in MATRIX [55] is applicable to any final state with two charged leptons and two neutrinos, but in this paper we will focus on the different-flavour signature $\mu^+e^-\nu_\mu\bar{\nu}_e$. The impact of QCD corrections on cross sections and distributions will be studied both at inclusive level and in presence of typical experimental selection cuts for W^+W^- measurements and $H \to W^+W^-$ studies. The presented NNLO results for fiducial cross sections and for the efficiencies of the corresponding acceptance cuts provide first insights into acceptance efficiencies and jet-veto effects at NNLO.

As pointed out in Ref. [46], radiative QCD corrections resulting from real bottom-quark emissions lead to a severe contamination of W-pair production through top-quark resonances in the W^+W^-b and $W^+W^-b\bar{b}$ channels. The enhancement of the W^+W^- cross section that results from the opening of the $t\bar{t}$ channel at NNLO can exceed a factor of five. It is thus clear that a careful subtraction of $t\bar{t}$ and single-top contributions is indispensable in order to ensure a decent convergence of the perturbative series. To this end, we adopt a top-free definition of the W^+W^- cross section based on a complete bottom-quark veto in the four-flavour scheme. The uncertainty related with this prescription will be assessed by means of an alternative top-subtraction approach based on the top-quark-width dependence of the W^+W^- cross section in the five-flavour scheme [46].

The manuscript is organized as follows. In Section 2 we describe technical aspects of the computation, including the subtraction of resonant top-quark contributions (Section 2.1), q_T subtraction (Section 2.2), the MATRIX framework (Section 2.3), and the stability of (N)NLO predictions based on q_T subtraction (Section 2.4). Section 3 describes our numerical results for $pp \to \mu^+e^-\nu_\mu\bar{\nu}_e + X$: We present the input parameters (Section 3.1), cross sections and distributions without acceptance cuts (Section 3.2) and with cuts corresponding to W^+W^- signal (Section 3.3) and Higgs analyses (Section 3.4). The main results are summarized in Section 4.

2 Description of the calculation

We study the process

$$pp \to l^+l'^-\nu_l\bar{\nu}_{l'} + X, \tag{1}$$

including all resonant and non-resonant Feynman diagrams that contribute to the production of two charged leptons and two neutrinos.

Depending on the flavour of the final-state leptons, the generic reaction in Eq. (1) can involve different combinations of vector-boson resonances. The different-flavour final state $l^+l'^-\nu_l\bar{\nu}_{l'}$ is generated, as shown in Figure 1 for the $q\bar{q}$ process at LO,

(a) via resonant t-channel W^+W^- production with subsequent $W^+ \to l^+\nu_l$ and $W^- \to l'^-\bar{\nu}_{l'}$ decays;

(b) via s-channel production in $Z^{(*)}/\gamma^* \to WW^{(*)}$ topologies through a triple-gauge-boson vertex with subsequent $W^+ \to l^+\nu_l$ and $W^- \to l'^-\bar{\nu}_{l'}$ decays, where either both W bosons, or the Z boson and one of the W bosons can become simultaneously resonant;

(c) via Z/γ^* production with a subsequent decay $Z/\gamma^* \to l\nu_l W \to ll'\nu_l\nu_{l'}$. Note that kinematics again allows for a resonant W boson in the decay chain of a resonant Z boson.

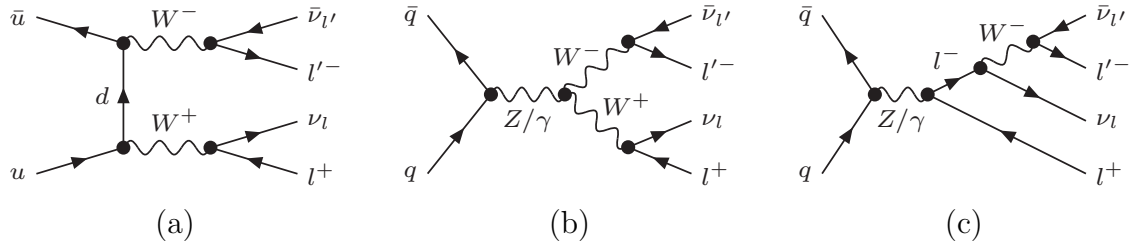

Figure 1: Sample of Born diagrams contributing to W^+W^- production both in the different-flavour case ($l \neq l'$) and in the same-flavour case ($l = l'$).

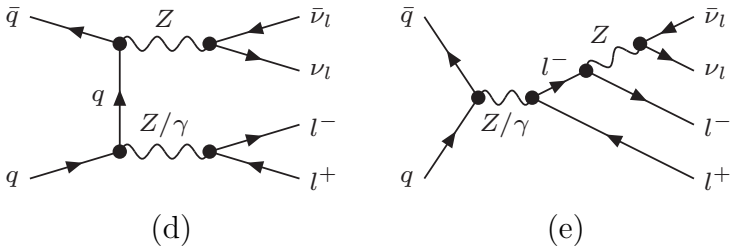

Figure 2: Sample of Born diagrams contributing to W^+W^- production only in the same-flavour case. In the different-flavour case, they would describe ZZ production in the $2l2\nu'$ channel.

Additionally, in the case of equal lepton flavours, $l = l'$, off-shell ZZ production diagrams are involved, as shown in Figure 2, where the $l^+l^-\nu_l\bar{\nu}_l$ final state is generated

(d) via resonant t-channel ZZ production with $Z \to l^+l^-$ and $Z \to \nu_l\bar{\nu}_l$ decays;

(e) via further $Z \to 4$ leptons topologies, $Z/\gamma^* \to llZ \to ll\nu_l\nu_l$ or $Z \to \nu_l\nu_l Z \to ll\nu_l\nu_l$. Any double-resonant configurations are kinematically suppressed or excluded by phase-space cuts.

Note that the appearance of infrared (IR) divergent $\gamma^* \to l^+l^-$ splittings in the case of equal lepton flavours would prevent a fully inclusive phase-space integration.

Our calculation is performed in the complex-mass scheme [54], and besides resonances, it includes also contributions from off-shell EW bosons and all relevant interferences; no resonance approximation is applied. Our implementation can deal with any combination of leptonic flavours, $l, l' \in \{e, \mu, \tau\}$. However, in this paper we will focus on the different-flavour channel $pp \to \mu^+e^-\nu_\mu\bar{\nu}_e + X$. For the sake of brevity, we will often denote this process as W^+W^- production though.

The NNLO computation requires the following scattering amplitudes at $\mathcal{O}(\alpha_S^2)$:

- tree amplitudes for $q\bar{q} \to l^+l'^-\nu_l\bar{\nu}_{l'}\,gg$, $q\bar{q}^{(\prime)} \to l^+l'^-\nu_l\bar{\nu}_{l'}\,q^{(\prime\prime)}\bar{q}^{(\prime\prime\prime)}$, and crossing-related processes;
- one-loop amplitudes for $q\bar{q} \to l^+l'^-\nu_l\bar{\nu}_{l'}\,g$, and crossing-related processes;
- squared one-loop amplitudes for $q\bar{q} \to l^+l'^-\nu_l\bar{\nu}_{l'}$ and $gg \to l^+l'^-\nu_l\bar{\nu}_{l'}$;
- two-loop amplitudes for $q\bar{q} \to l^+l'^-\nu_l\bar{\nu}_{l'}$.

All required tree-level and one-loop amplitudes are obtained from the OpenLoops generator [57,58], which implements a fast numerical recursion for the calculation of NLO scattering amplitudes within the Standard Model. For the numerically stable evaluation of tensor integrals we employ the Collier library [67–69], which is based on the Denner–Dittmaier reduction techniques [70, 71] and the scalar integrals of Ref. [72]. For the two-loop helicity amplitudes we rely on a public C++ library [73] that implements the results of Ref. [48], and for the numerical evaluation of the relevant multiple polylogarithms we use the implementation [74] in the GiNaC [75] library. The contribution of the massive-quark loops is neglected in the two-loop amplitudes, but accounted for anywhere else, in particular in the loop-induced gg channel.

2.1 W^+W^- contamination through single-top and $t\bar{t}$ production

The theoretical description of W^+W^- production at higher orders in QCD is complicated by a subtle interplay with top-production processes, which originates from real-emission channels with final-state bottom quarks [38, 45, 46]. In the five-flavour scheme (5FS), where bottom quarks are included in the parton-distribution functions and the bottom-quark mass is set to zero, the presence of real bottom-quark emission is essential to cancel collinear singularities that arise from $g \to b\bar{b}$ splittings in the virtual corrections. At the same time, the occurrence of Wb pairs in the real-emission matrix elements induces $t \to Wb$ resonances that lead to a severe contamination of W^+W^- production. The problem starts with the NLO cross section, which receives a single-resonant $tW \to W^+W^-b$ contribution of about 30% (60%) at 7 (14) TeV. At NNLO, the appearance of double-resonant $t\bar{t} \to W^+W^-b\bar{b}$ production channels enhances the W^+W^- cross section by about a factor of four (eight) [46]. Such single-top and $t\bar{t}$ contributions arise through the couplings of W bosons to external bottom quarks and enter at the same orders in α and α_S as (N)NLO QCD contributions from light quarks. Their huge impact jeopardises the convergence of the perturbative expansion. Thus, precise theoretical predictions for W^+W^- production require a consistent prescription to subtract the top contamination.

In principle, resonant top contributions can be suppressed by imposing a b-jet veto, similarly as in experimental analyses. However, for a b-jet veto with typical p_T values of $20 - 30\,\text{GeV}$, the top contamination remains as large as about 10% [46], while in the limit of a vanishing b-jet veto p_T's the NLO and NNLO W^+W^- cross sections suffer from collinear singularities associated with massless bottom quarks in the 5FS.

To circumvent this problem, throughout this paper we use the four-flavour scheme (4FS), where the bottom mass renders all partonic subprocesses with bottom quarks in the final state separately finite. In this scheme, the contamination from $t\bar{t}$ and single-top production is easily avoided by omitting bottom-quark emission subprocesses. However, this prescription generates logarithms of the bottom mass that could have a non-negligible impact on the W^+W^- cross section. In order to assess the related uncertainty, results in the 4FS are compared against a second calculation in the 5FS. In that case, the contributions that are free from top resonances are isolated with a gauge-invariant approach that exploits the scaling behaviour of the cross sections in the limit of a vanishing top-quark width [46]. The idea is that double-resonant (single-resonant) contributions depend quadratically (linearly) on $1/\Gamma_t$, while top-free W^+W^- contributions are not enhanced at small Γ_t. Exploiting this scaling property, the $t\bar{t}$, tW and (top-free) W^+W^- components in the 5FS are separated from each other through a numerical fit based on multiple high-statistics

evaluations of the cross section for increasingly small values of Γ_t. The subtracted result in the 5FS can then be understood as a theoretical prediction of the genuine W^+W^- cross section and directly compared to the 4FS result. The difference should be regarded as an ambiguity in the definition of a top-free W^+W^- cross section and includes, among other contributions, the quantum interference between W^+W^- production (plus unresolved bottom quarks) and $t\bar{t}$ or single-top production. This ambiguity was shown to be around $1\% - 2\%$ for the inclusive W^+W^- cross section at NNLO [46], and turns out to be of the same size or even smaller in presence of a jet veto (see Section 3).

2.2 The q_T-subtraction formalism

The implementation of the various IR-divergent amplitudes into a numerical code that provides finite NNLO predictions for physical observables is a highly non-trivial task. In particular, the numerical computations need to be arranged in a way that guarantees the cancellation of IR singularities across subprocesses with different parton multiplicities. To this end various methods have been developed. They can be classified in two broad categories. In the first one, the NNLO calculation is organized so as to cancel IR singularities of both NLO and NNLO type at the same time. The formalisms of antenna subtraction [76–79], colourful subtraction [80–82] and Stripper [83–85] belong to this category. Antenna subtraction and colourful subtraction can be considered as extensions of the NLO subtraction methods of Refs. [86–89] to NNLO. Stripper, instead, is a combination of the FKS subtraction method [86] with numerical techniques based on sector decomposition [90, 91]. The methods in the second category start from an NLO calculation with one additional parton (jet) in the final state and devise suitable subtractions to make the cross section finite in the region in which the additional parton (jet) leads to further divergences. The q_T-subtraction method [59] as well as N-jettiness subtraction [92–94], and the Born-projection method of Ref. [95] belong to this class.

The q_T-subtraction formalism [59] has been conceived in order to deal with the production of any colourless[†] high-mass system F at hadron colliders. This method has already been applied in several NNLO calculations [46, 59, 62–66, 97–100], and we have employed it also to obtain the results presented in this paper. In the q_T-subtraction framework, the $pp \to F + X$ cross section at (N)NLO can be written as

$$\mathrm{d}\sigma^{\mathrm{F}}_{\mathrm{(N)NLO}} = \mathcal{H}^{\mathrm{F}}_{\mathrm{(N)NLO}} \otimes \mathrm{d}\sigma^{\mathrm{F}}_{\mathrm{LO}} + \left[\mathrm{d}\sigma^{\mathrm{F+jet}}_{\mathrm{(N)LO}} - \mathrm{d}\sigma^{\mathrm{CT}}_{\mathrm{(N)NLO}}\right]. \tag{2}$$

The term $d\sigma^{\mathrm{F+jet}}_{\mathrm{(N)LO}}$ represents the cross section for the production of the system F plus one jet at (N)LO accuracy and can be evaluated with any available NLO subtraction formalism. The counterterm $\mathrm{d}\sigma^{\mathrm{CT}}_{\mathrm{(N)NLO}}$ guarantees the cancellation of the remaining IR divergences of the F+jet cross section. It is obtained via fixed-order expansion from the resummation formula for logarithmically enhanced contributions at small transverse momenta [60]. The practical implementation of the contributions in the square bracket in Eq. (2) is described in more detail in Section 2.3.

The hard-collinear coefficient $\mathcal{H}^{\mathrm{F}}_{\mathrm{(N)NLO}}$ encodes the loop corrections to the Born-level process

[†]The extension to heavy-quark production has been discussed in Ref. [96].

and compensates[‡] for the subtraction of $\mathrm{d}\sigma^{\mathrm{CT}}_{(\mathrm{N})\mathrm{NLO}}$. It is obtained from the (N)NLO truncation of the process-dependent perturbative function

$$\mathcal{H}^{\mathrm{F}} = 1 + \frac{\alpha_{\mathrm{S}}}{\pi}\,\mathcal{H}^{\mathrm{F}(1)} + \left(\frac{\alpha_{\mathrm{S}}}{\pi}\right)^2 \mathcal{H}^{\mathrm{F}(2)} + \dots \quad . \tag{3}$$

The NLO calculation of $\mathrm{d}\sigma^{\mathrm{F}}$ requires the knowledge of $\mathcal{H}^{\mathrm{F}(1)}$, and the NNLO calculation also requires $\mathcal{H}^{\mathrm{F}(2)}$. The general structure of $\mathcal{H}^{\mathrm{F}(1)}$ has been known for a long time [101]. Exploiting the explicit results of $\mathcal{H}^{\mathrm{F}(2)}$ for Higgs [102] and vector-boson [103] production, the result of Ref. [101] has been extended to the calculation of the NNLO coefficient $\mathcal{H}^{\mathrm{F}(2)}$ [104]. These results have been confirmed through an independent calculation in the framework of Soft–Collinear Effective Theory [105, 106]. The counterterm $\mathrm{d}\sigma^{\mathrm{CT}}_{(\mathrm{N})\mathrm{NLO}}$ only depends on $\mathcal{H}^{\mathrm{F}}_{(\mathrm{N})\mathrm{LO}}$, i.e. for an NNLO computation it requires only $\mathcal{H}^{\mathrm{F}(1)}$ as input, which can be derived from the one-loop amplitudes for the Born subprocesses.

2.3 Organization of the calculation in Matrix

Our calculation of W^+W^- production is based on Matrix [55], a widely automated program for NNLO calculations at hadron colliders. This new tool is based on q_T subtraction, and is thus applicable to any process with a colourless high-mass final state, provided that the two-loop amplitudes for the Born subprocess are available. Moreover, besides fixed-order calculations, it supports also the resummation of logarithmically enhanced terms at NNLL accuracy (see Ref. [53], and Ref. [107] for more details).

Matrix is based on Munich [56], a general-purpose Monte Carlo program that includes a fully automated implementation of the Catani–Seymour dipole subtraction method [88, 89], an efficient phase-space integration, as well as an interface to the one-loop generator OpenLoops [57, 58] to obtain all required (spin- and colour-correlated) tree-level and one-loop amplitudes. Munich takes care of the bookkeeping of all relevant partonic subprocesses. For each subprocess it automatically generates adequate phase-space parameterizations based on the resonance structure of the underlying (squared) tree-level Feynman diagrams. These parameterizations are combined using a multi-channel approach to simultaneously flatten the resonance structure of the amplitudes, and thus guarantee a fast convergence of the numerical integration. Several improvements like an adaptive weight-optimization procedure are implemented as well.

Supplementing the fully automated NLO framework of Munich with a generic implementation of the q_T-subtraction and -resummation techniques, Matrix achieves NNLL+NNLO accuracy in a way that limits the additionally introduced dependence on the process to the two-loop amplitudes that enter $\mathcal{H}^{\mathrm{F}}_{\mathrm{NNLO}}$ in Eq. (2). All other process-dependent information entering the various ingredients in Eq. (2) are expressed in terms of NLO quantities already available within Munich+OpenLoops.

All NNLO contributions with vanishing total transverse momentum q_T of the final-state system F are collected in the coefficient $\mathcal{H}^{\mathrm{F}}_{\mathrm{NNLO}}$. The remaining part of the NNLO cross section, namely the difference in the square bracket in Eq. (2), is formally finite in the limit $q_T \to 0$, but each

[‡]More precisely, while the behaviour of $\mathrm{d}\sigma^{\mathrm{CT}}_{(\mathrm{N})\mathrm{NLO}}$ for $q_T \to 0$ is dictated by the singular structure of $d\sigma^{\mathrm{F+jet}}_{(\mathrm{N})\mathrm{LO}}$, its non-divergent part in the same limit is to some extent arbitrary, and its choice determines the explicit form of $\mathcal{H}^{\mathrm{F}}_{(\mathrm{N})\mathrm{NLO}}$.

term separately exhibits logarithmic divergences in this limit. Since the subtraction is non-local, a technical cut on q_T is introduced in order to render both terms separately finite. In this way, the q_T-subtraction method works very similarly to a phase-space slicing method. In practice, it turns out to be more convenient to use a cut, r_{cut}, on the dimensionless quantity $r = q_T/M$, where M denotes the invariant mass of the final-state system F.

The counterterm $\mathrm{d}\sigma^{\text{CT}}_{\text{(N)NLO}}$ cancels all divergent terms from the real-emission contributions at small q_T, implying that the r_{cut} dependence of their difference should become numerically negligible for sufficiently small values of r_{cut}. In practice, as both the counterterm and the real-emission contribution grow arbitrarily large for $r_{\text{cut}} \to 0$, the statistical accuracy of the Monte Carlo integration degrades, preventing one from pushing r_{cut} too low. In general, the absence of any strong residual r_{cut} dependence provides a stringent check on the correctness of the computation since any significant mismatch between the contributions would result in a divergent cross section in the limit $r_{\text{cut}} \to 0$. To monitor the r_{cut} dependence without the need of repeated CPU-intensive runs, MATRIX allows for simultaneous cross-section evaluations at variable r_{cut} values. The numerical information on the r_{cut} dependence of the cross section can be used to quantify the uncertainty due to finite r_{cut} values (see Section 2.4).

2.4 Stability of q_T subtraction for $\mu^+e^-\nu_\mu\bar{\nu}_e$ production

In the following we investigate the stability of the q_T subtraction approach for $pp \to \mu^+e^-\nu_\mu\bar{\nu}_e + X$. To this end, in Figure 3 we plot the NLO and NNLO cross sections as functions of the q_T-subtraction cut, r_{cut}, which acts on the dimensionless variable $r = p_{T,\mu^+e^-\nu_\mu\bar{\nu}_e}/m_{\mu^+e^-\nu_\mu\bar{\nu}_e}$. Validation plots are presented at 8 TeV both for the fully inclusive cross section (see Section 3.2) and for the most exclusive case we have investigated, i.e. the cross section in presence of standard fiducial cuts for Higgs background analyses (see Section 3.4). All considered scenarios at 8 and 13 TeV lead essentially to the same conclusions.

At NLO the r_{cut}-independent cross section obtained with Catani–Seymour subtraction is used as a reference for the validation of the q_T-subtraction result. The comparison of the NLO cross sections in the left panels of Figure 3 demonstrates that q_T subtraction reaches about half-permille accuracy already at the moderate value of $r_{\text{cut}} = 1\%$, where we can, however, still resolve a difference, which is slightly larger than the respective numerical uncertainties, with respect to the r_{cut}-independent result achieved using Catani–Seymour subtraction. This difference is due to the well-known power-suppressed contributions that are left after the cancellation of the logarithmic singularity at small r_{cut}. Going to even smaller values of r_{cut}, we observe a perfect convergence within statistical uncertainties towards the Catani–Seymour-subtracted result in the limit $r_{\text{cut}} \to 0$.

At NNLO, where an r_{cut}-independent control result is not available, we observe no significant, i.e. beyond the numerical uncertainties, r_{cut} dependence below about $r_{\text{cut}} = 1\%$; we thus use the finite-r_{cut} results to extrapolate to $r_{\text{cut}} = 0$, taking into account the breakdown of predictivity for very low r_{cut} values, and conservatively assign an additional numerical error to our results due to this extrapolation. This procedure allows us to control all NNLO predictions to inclusive and fiducial cross sections presented in Section 3 well below the level of two per mille. The increasing error bars indicate that arbitrarily low r_{cut} values cannot be tested as the contributions cancelling in the limit are separately divergent.

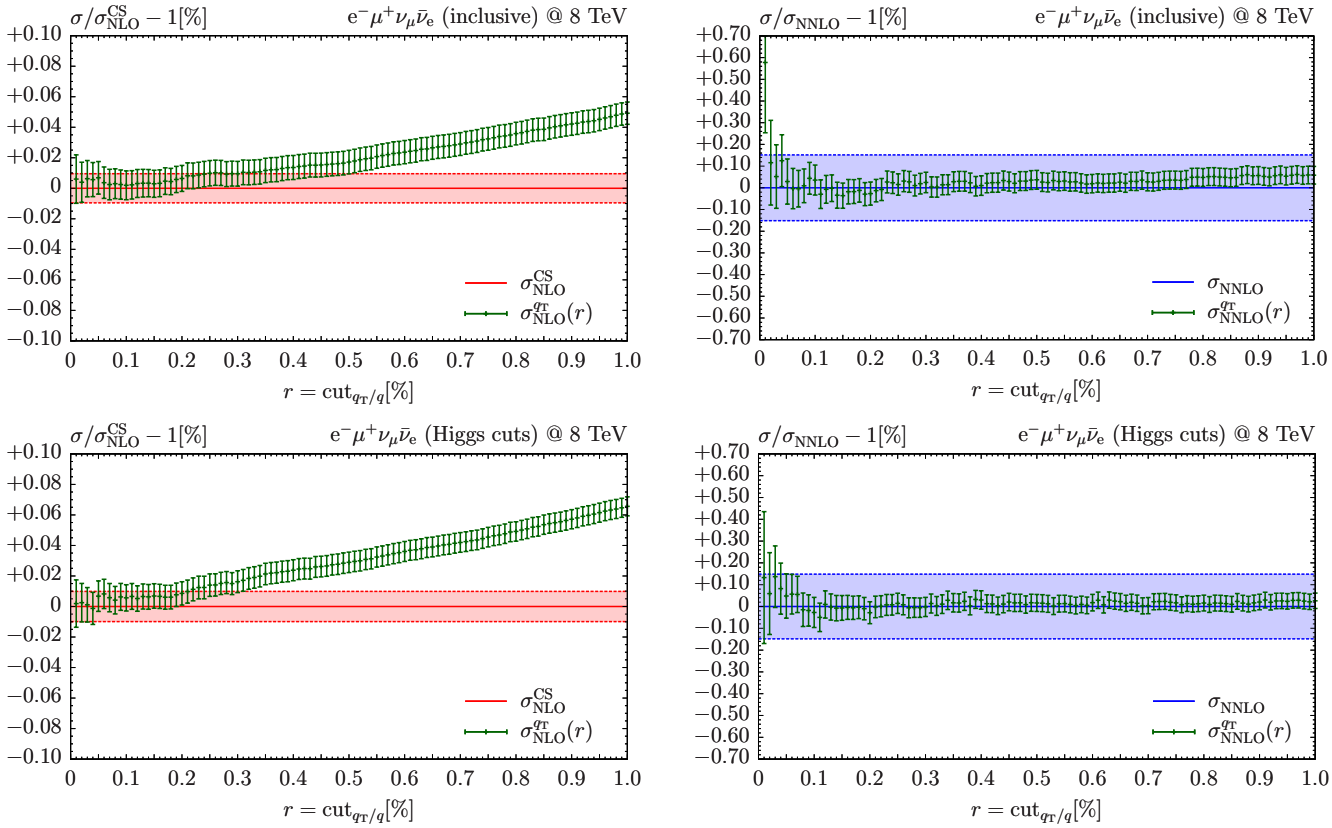

Figure 3: Dependence of the $pp \to \mu^+ e^- \nu_\mu \bar{\nu}_e + X$ cross sections at 8 TeV on the q_T-subtraction cut, $r_{\rm cut}$, for both NLO (left plots) and NNLO (right plots) results in the inclusive phase space (upper plots) and with Higgs cuts (lower plots). NLO results are normalized to the $r_{\rm cut}$-independent NLO cross section computed with Catani–Seymour subtraction, and the NNLO results are normalized to their values at $r_{\rm cut} \to 0$, with a conservative extrapolation-error indicated by the blue bands.

Based on the observation that no significant $r_{\rm cut}$ dependence is found below $r_{\rm cut} = 1\%$, the value $r_{\rm cut} = 0.25\%$ was adopted for the calculation of the differential observables presented in Section 3. We have checked that the total rates for that value are fully consistent within numerical uncertainties with our extrapolated results and that a smaller value $r_{\rm cut} = 0.1\%$ leads to distributions in full statistical agreement, thus confirming the robustness of our results also at the differential level.

3 Results

We present numerical results for the different-flavour process $pp \to \mu^+ e^- \nu_\mu \bar{\nu}_e + X$ at $\sqrt{s} = 8\,\text{TeV}$ and 13 TeV. Cross sections and distributions are studied both in the inclusive phase space and in presence of typical selection cuts for W^+W^- and $H \to W^+W^-$ analyses.

Different-flavour final states provide the highest sensitivity both in W^+W^- measurements and Higgs studies. We note that, due to the charge asymmetry of W^+W^- production in proton–proton collisions and the differences in the muon and electron acceptance cuts (in particular regarding the

rapidity cuts), the two different-flavour channels, $\mu^+e^-\nu_\mu\bar{\nu}_e$ and $e^+\mu^-\nu_e\bar{\nu}_\mu$, do not yield identical cross sections. However, we have checked that the absolute differences are not resolved on the level of our statistical errors. Thus (N)NLO predictions and K-factors for $\mu^+e^-\nu_\mu\bar{\nu}_e$ production can be safely applied also to $pp \to e^+\mu^-\nu_e\bar{\nu}_\mu + X$.

3.1 Input parameters, PDFs and selection cuts

Results in this paper are based on the EW input parameters $G_\mu = 1.1663787 \times 10^{-5}$ GeV^{-2}, $m_W = 80.385$ GeV and $m_Z = 91.1876$ GeV. The other couplings in the EW sector are derived in the G_μ-scheme, where $\cos\theta_\mathrm{w} = m_W/m_Z$ and $\alpha = \sqrt{2}G_\mu m_W^2 \sin^2\theta_\mathrm{w}/\pi$. In the complex-mass scheme, the physical gauge-boson masses and the weak mixing angle are replaced by $\mu_V = \sqrt{m_V^2 - \mathrm{i}\Gamma_V m_V}$ and $\cos\hat{\theta}_\mathrm{w} = \mu_W/\mu_Z$, while for α the above real-valued expression is used. For the vector-boson widths we employ $\Gamma_W = 2.085$ GeV and $\Gamma_Z = 2.4952$ GeV [108], and for the heavy quarks we set $m_b = 4.92$ GeV and $m_t = 172.5$ GeV. These input parameters result in a branching fraction $\mathrm{BR}(W^\pm \to l^\pm\nu_l) = 0.1090040$ for each massless lepton generation, i.e. $l = e, \mu$. Contributions from resonant Higgs bosons and their interference with the W^+W^- continuum are fully supported in our implementation. However, since this study is focused on W^+W^- production as EW signal or as background to $H \to W^+W^-$, Higgs contributions have been decoupled by taking the $m_H \to \infty$ limit.

To compute hadronic cross sections, we use NNPDF3.0 parton-distribution functions (PDFs) [109], and, unless stated otherwise, we work in the 4FS, while removing all contributions with final-state bottom quarks in order to avoid any contamination from top-quark resonances. In the NNPDF framework, 4FS PDFs are derived from the standard variable-flavour-number PDF set with $\alpha_s^{(5\mathrm{F})}(M_Z) = 0.118$ via appropriate backward and forward evolution with five and four active flavours, respectively. The resulting values of the strong coupling $\alpha_s^{(4\mathrm{F})}(M_Z)$ at LO, NLO and NNLO are 0.1136, 0.1123 and 0.1123, respectively. Predictions at N^{n}LO are obtained using PDFs at the corresponding perturbative order and the evolution of α_S at $(n+1)$-loop order, as provided by the PDF set. The central values of the factorization and renormalization scales are set to $\mu_F = \mu_R = m_W$. Scale uncertainties are estimated by varying μ_F and μ_R in the range $0.5\,m_W \le \mu_F, \mu_R \le 2\,m_W$ with the restriction $0.5 \le \mu_F/\mu_R \le 2$.

In the following subsections we investigate $\mu^+e^-\nu_\mu\bar{\nu}_e$ production in the inclusive phase space (Section 3.2) and in presence of typical selection cuts that are designed for measurements of W^+W^- production (Section 3.3) and for $H \to W^+W^-$ studies (Section 3.4) at the LHC. The detailed list of cuts is specified in Table 1. Besides the requirement of two charged leptons within a certain transverse-momentum and rapidity region, they involve additional restrictions on the missing transverse momentum ($p_T^\mathrm{miss} = p_{T,\nu\bar{\nu}}$), the transverse momentum ($p_{T,ll}$) and invariant mass (m_{ll}) of the dilepton system, the combined rapidity–azimuth (ΔR_{ll}) and azimuthal ($\Delta\phi_{ll}$) separation of the charged leptons, as well as on the relative missing transverse momentum ($p_T^\mathrm{miss,rel}$) and the azimuthal angle between $\mathbf{p_{T,ll}}$, and $\mathbf{p_T^\mathrm{miss}}$ ($\Delta\phi_{ll,\nu\nu}$), as defined in Table 1. Moreover, the W^+W^- and Higgs selection criteria involve a veto against anti-k_T jets [110] with $R = 0.4$, $p_T > 25\,\mathrm{GeV}$ and $|y| < 4.5$.

cut variable	W^+W^- cuts	Higgs cuts
lepton definition		
p_{T,l_1}	$> 25\,\text{GeV}$	$> 22\,\text{GeV}$
p_{T,l_2}	$> 20\,\text{GeV}$	$> 10\,\text{GeV}$
$\lvert y_\mu \rvert$	< 2.4	< 2.4
$\lvert y_e \rvert$	< 2.47 and $\notin [1.37; 1.52]$	< 2.47 and $\notin [1.37; 1.52]$
leptonic cuts		
p_T^{miss}	$> 20\,\text{GeV}$	$> 20\,\text{GeV}$
$p_T^{\text{miss,rel}}$	$> 15\,\text{GeV}$	—
$p_{T,ll}$	—	$> 30\,\text{GeV}$
m_{ll}	$> 10\,\text{GeV}$	$\in [10\,\text{GeV}; 55\,\text{GeV}]$
ΔR_{ll}	> 0.1	—
$\Delta\phi_{ll}$	—	< 1.8
$\Delta\phi_{ll,\nu\nu}$	—	$> \pi/2$
anti-k_T jets with $R = 0.4$, $p_{T,j} > 25\,\text{GeV}$, $\lvert y_j \rvert < 4.5$		
N_{jets}	0	0

Table 1: Selection cuts targeted at W^+W^- signal measurements (central column) and $H \to W^+W^-$ studies (right column). The hardest and second hardest lepton are denoted as l_1 and l_2, respectively. The missing transverse momentum, p_T^{miss}, is identified with the total transverse momentum of the $\nu\bar{\nu}$ pair, while the relative missing transverse momentum $p_T^{\text{miss,rel}}$ is defined as $p_T^{\text{miss}} \times \sin|\Delta\phi|$, where $\Delta\phi$ is the azimuthal separation between $\mathbf{p_T^{\text{miss}}}$ and the momentum of the closest lepton; $\Delta\phi_{ll,\nu\nu}$ is the azimuthal angle between the vectorial sum of the leptons' transverse momenta, $\mathbf{p_{T,ll}}$, and $\mathbf{p_T^{\text{miss}}}$.

3.2 Analysis of inclusive $\mu^+e^-\nu_\mu\bar{\nu}_e$ production

In this Section we study $\mu^+e^-\nu_\mu\bar{\nu}_e$ production in absence of acceptance cuts. Predictions for the total inclusive cross section at LO, NLO and NNLO are listed in Table 2. The NLO cross section computed with NNLO PDFs, denoted by NLO′, and NLO′ supplemented with the loop-induced gluon-fusion contribution (NLO′+gg) are provided as well.

At $\sqrt{s} = 8\,(13)\,\text{TeV}$ the NLO corrections increase the LO cross section by 47% (55%), and the NNLO corrections result in a further sizeable shift of +11% (+14%) with respect to NLO. The total NNLO correction can be understood as the sum of three contributions that can be read off Table 2: Evaluating the cross section up to $\mathcal{O}(\alpha_S)$ with NNLO PDFs increases the NLO result by about 2% (3%). The loop-induced gluon-fusion channel, which used to be considered the dominant part of the NNLO corrections, further raises the cross section by only 3% (4%), while the genuine

	$\sigma_{\text{inclusive}}$ [fb]		$\sigma/\sigma_{\text{NLO}} - 1$	
$\sqrt{s}$	8 TeV	13 TeV	8 TeV	13 TeV
LO	$425.41(4)\,^{+2.8\%}_{-3.6\%}$	$778.99\ (8)\,^{+5.7\%}_{-6.7\%}$	-31.8%	-35.4%
NLO	$623.47(6)\,^{+3.6\%}_{-2.9\%}$	$1205.11(12)\,^{+3.9\%}_{-3.1\%}$	0	0
NLO′	$635.95(6)\,^{+3.6\%}_{-2.8\%}$	$1235.82(13)\,^{+3.9\%}_{-3.1\%}$	$+\ 2.0\%$	$+\ 2.5\%$
NLO′+gg	$655.83(8)\,^{+4.3\%}_{-3.3\%}$	$1286.81(13)\,^{+4.8\%}_{-3.7\%}$	$+\ 5.2\%$	$+\ 6.8\%$
NNLO	$690.4(5)\ \ ^{+2.2\%}_{-1.9\%}$	$1370.9(11)\ \ ^{+2.6\%}_{-2.3\%}$	$+10.7\%$	$+13.8\%$

Table 2: Total inclusive cross sections at different perturbative orders and relative differences with respect to NLO. The quoted uncertainties correspond to scale variations as described in the text, and the numerical integration errors on the previous digit(s) are stated in brackets; for the NNLO results, the latter include the uncertainty due the r_{cut} extrapolation (see Section 2.4).

$\mathcal{O}(\alpha_{\text{S}}^2)$ corrections to the $q\bar{q}$ channel[§] amount to about +6% (+7%). Neglecting PDF effects, we find that the loop-induced gg contribution corresponds to only 37% (38%) of the total $\mathcal{O}(\alpha_{\text{S}}^2)$ effect, i.e. of $\sigma_{\text{NNLO}} - \sigma_{\text{NLO}'}$, with the remaining 63% (62%) being due to genuine NNLO corrections.

These results are in line with the inclusive on-shell predictions of Ref. [46], where the relative weight of the gg contribution was found to be 35% (36%), and the small difference is due to the chosen PDFs. We also find by up to about 2% larger NNLO corrections than stated in Ref. [46], which can also be attributed to the chosen PDF sets. Indeed, repeating the on-shell calculation of Ref. [46] using the input parameters of Section 3.1 (with $\Gamma_W = \Gamma_Z = 0$), we find that the relative corrections agree on the level of the statistical error when the same PDF sets are applied. Moreover, comparing the results of Table 2 with this on-shell calculation allows us to quantify the size of off-shell effects, which turn out to reduce the on-shell result by about 2% with a very mild dependence (at the permille level) on the perturbative order and the collider energy. The results for the two considered collider energies confirm that the size of relative corrections slightly increases with the centre-of-mass energy, as in the on-shell case.

We add a few comments on the theoretical uncertainties of the above results. As is well known, scale variations do not give a reliable estimate of the size of missing higher-order contributions at the first orders of the perturbative expansion. In fact, LO and NLO predictions are not consistent within scale uncertainties, and the same conclusion can be drawn by comparing NLO or NLO′+gg predictions with their respective scale uncertainties to the central NNLO result. This can be explained by the fact that the qg (as well as $\bar{q}g$) and gg (as well as $qq^{(\prime)}$, $\bar{q}\bar{q}^{(\prime)}$ and $q\bar{q}'$) channels open up only at NLO and NNLO, respectively. Since the NNLO is the first order where all the partonic channels are contributing, the NNLO scale dependence should provide a realistic estimate of the uncertainty from missing higher-order corrections. The loop-induced gluon–gluon channel, which

[§]Here and in what follows, all NNLO corrections that do not stem from the loop-induced $gg \to W^+W^-$ channel are denoted as genuine $\mathcal{O}(\alpha_{\text{S}}^2)$ corrections or NNLO corrections to the $q\bar{q}$ channel. Besides $q\bar{q}$-induced partonic processes, they actually contain also gq and $g\bar{q}$ channels with one extra final-state parton as well as gg, $qq^{(\prime)}$, $\bar{q}\bar{q}^{(\prime)}$ and $q\bar{q}'$ channels with two extra final-state partons.

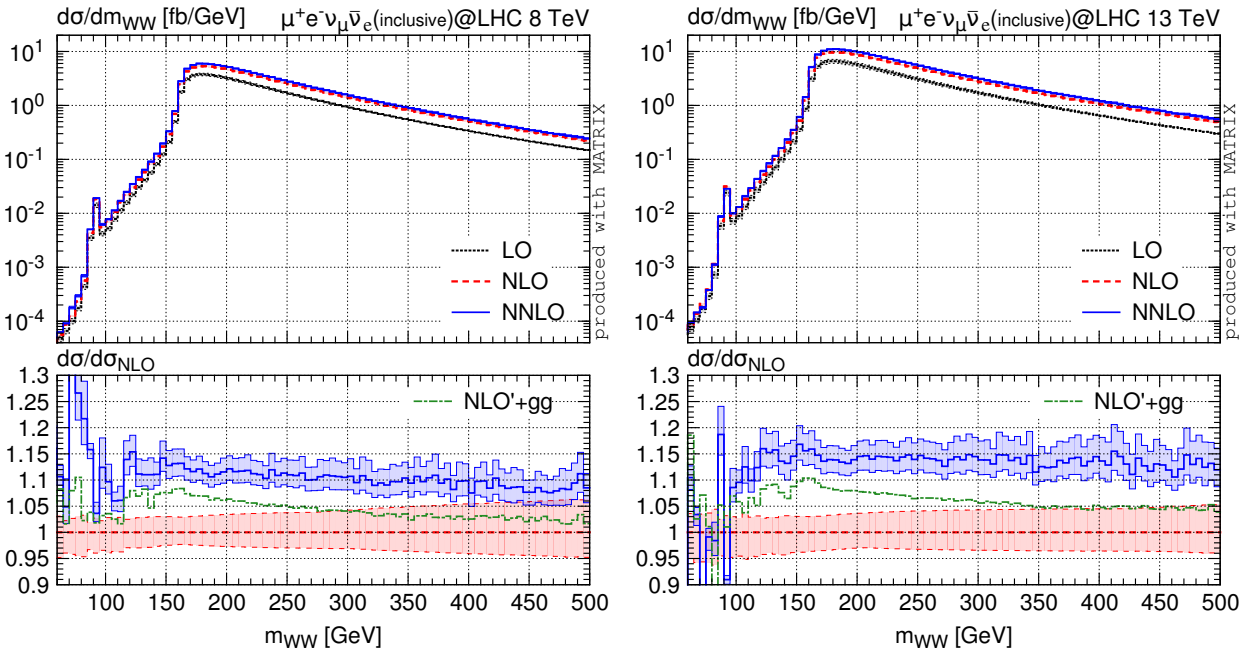

(a) (b)

Figure 4: Distribution in the invariant mass of the W^+W^- pair, $m_{W^+W^-} = m_{\mu^+e^-\nu_\mu\bar{\nu}_e}$. No acceptance cuts are applied. Absolute LO (black, dotted), NLO (red, dashed) and NNLO (blue, solid) predictions at $\sqrt{s} = 8\,\text{TeV}$ (left) and $\sqrt{s} = 13\,\text{TeV}$ (right) are plotted in the upper frames. The lower frames display NLO′+gg (green, dot-dashed) and NNLO predictions normalized to NLO. The bands illustrate the scale dependence of the NLO and NNLO predictions. In the case of ratios, scale variations are applied only to the numerator, while the NLO prediction in the denominator corresponds to the central scale.

contributes only at its leading order at $\mathcal{O}(\alpha_S^2)$ and thus could receive large relative corrections, was not expected to break this picture due to its overall smallness already in Ref. [46]. That conclusion is supported by the recent calculation of the NLO corrections to the loop-induced gg channel [37].

In Figures 4–7 we present distributions that characterize the kinematics of the reconstructed W bosons[¶]. Absolute predictions at the various perturbative orders are complemented by ratio plots that illustrate the relative differences with respect to NLO. In order to assess the importance of genuine NNLO corrections, full NNLO results are compared to NLO′+gg predictions in the ratio plots.

In Figure 4 we show the distribution in the total invariant mass, $m_{W^+W^-} = m_{\mu^+e^-\nu_\mu\bar{\nu}_e}$. This observable features the characteristic threshold behaviour around $2\,m_W$, with a rather long tail and a steeply falling cross section in the off-shell region below threshold. Although suppressed by two orders of magnitude, the Z-boson resonance that originates from topologies of type (b) and (c) in Figure 1 is clearly visible at $m_{\mu^+e^-\nu_\mu\bar{\nu}_e} = m_Z$. Radiative QCD effects turn out to be largely insensitive to the EW dynamics that governs off-shell W-boson decays and dictates the shape of

[¶]The various kinematic variables are defined in terms of the off-shell W-boson momenta, $p_{W^+} = p_{\mu^+} + p_{\nu_\mu}$ and $p_{W^-} = p_{e^-} + p_{\bar{\nu}_e}$.

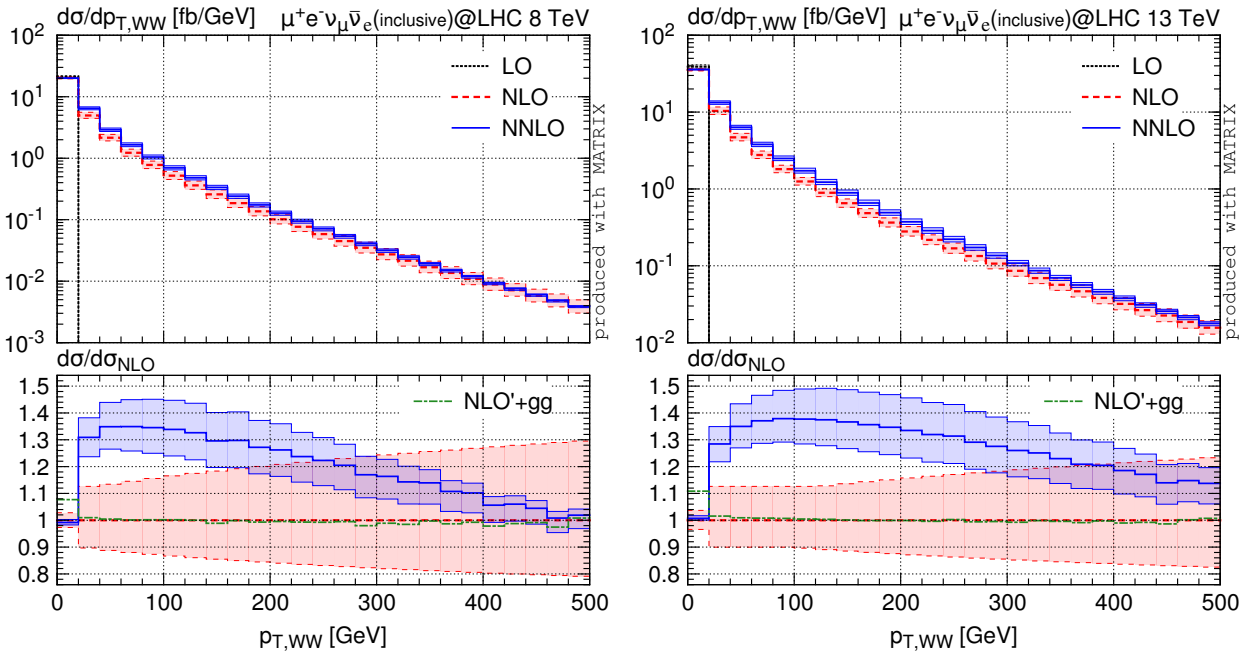

(a) (b)

Figure 5: Distribution in the transverse momentum of the W^+W^- pair. No acceptance cuts are applied. Absolute predictions and relative corrections as in Figure 4.

the $m_{\mu^+e^-\nu_\mu\bar{\nu}_e}$ distribution. In fact, the $\sigma_{\rm NNLO}/\sigma_{\rm NLO}$ ratio is rather flat, and shape distortions do not exceed about 5%, apart from the strongly suppressed region far below the $2\,m_W$ threshold.

The distribution in the transverse momentum of the W^+W^- pair, shown in Figure 5, vanishes at LO. Thus, at non-zero transverse momenta NLO (NNLO) results are formally only LO (NLO) accurate. Moreover, the loop-induced gg channel contributes only at $p_{T,WW} = 0$. The relative NNLO corrections are consistent with the results discussed in Ref. [53]: they are large and exceed the estimated scale uncertainties in the small and intermediate transverse-momentum regions, while the NLO and NNLO uncertainty bands overlap at large transverse momenta. At very low p_T, the fixed-order NNLO calculation diverges, but NNLL+NNLO resummation [53] can provide accurate predictions also in that region.

In Figures 6 and 7 the transverse-momentum distributions of the harder W boson, p_{T,W_1}, and the softer W boson, p_{T,W_2}, are depicted. The first eye-catching feature is the large NLO/LO correction in case of the harder W boson, which grows with p_T and leads to an enhancement by a factor of five at $p_T \approx 500\,\text{GeV}$, whereas such large corrections are absent for the softer W boson. This feature is due to the fact that the phase-space region with at least one hard W boson is dominantly populated by events with the NLO jet recoiling against this W boson, while the other W boson is relatively soft. The LO-like nature of this dominant contribution for moderate and large values of p_{T,W_1} is reflected by the large NLO scale band. The phase-space region where the softer W boson has moderate or high transverse momentum as well is naturally dominated by topologies with the two W bosons recoiling against each other. Such topologies are present already at LO, and thus do not result in exceptionally large corrections. Both for the leading

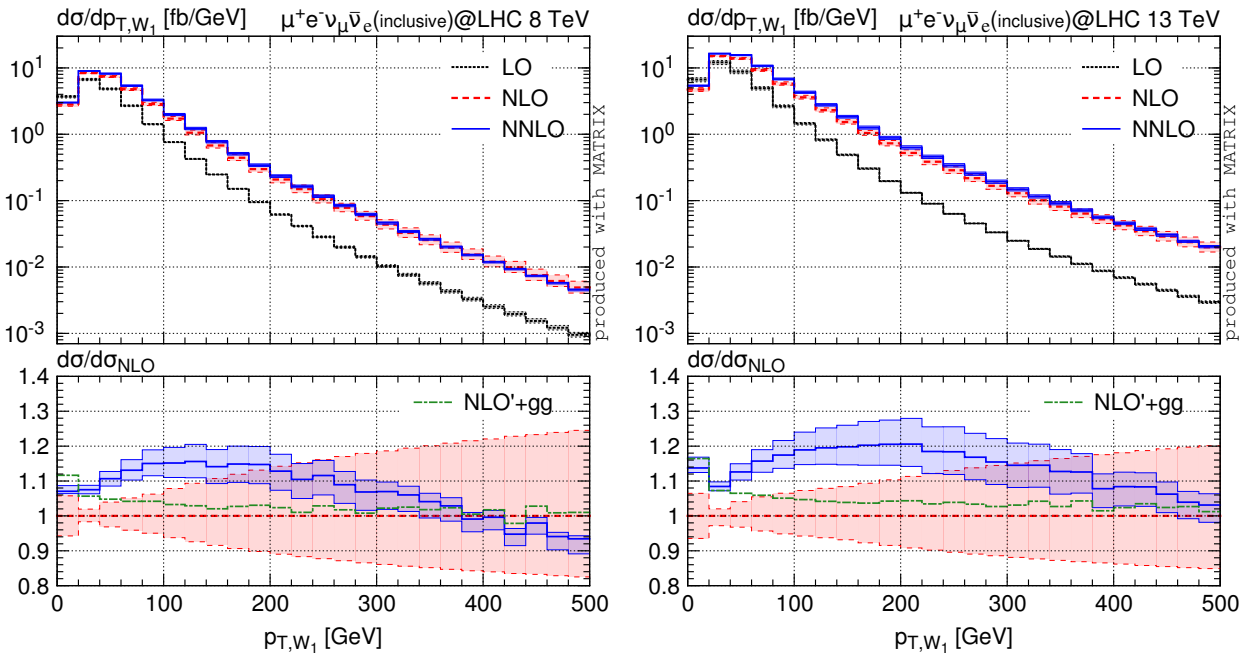

(a) (b)

Figure 6: Distribution in the transverse momentum of the harder reconstructed W boson. No acceptance cuts are applied. Absolute predictions and relative corrections as in Figure 4.

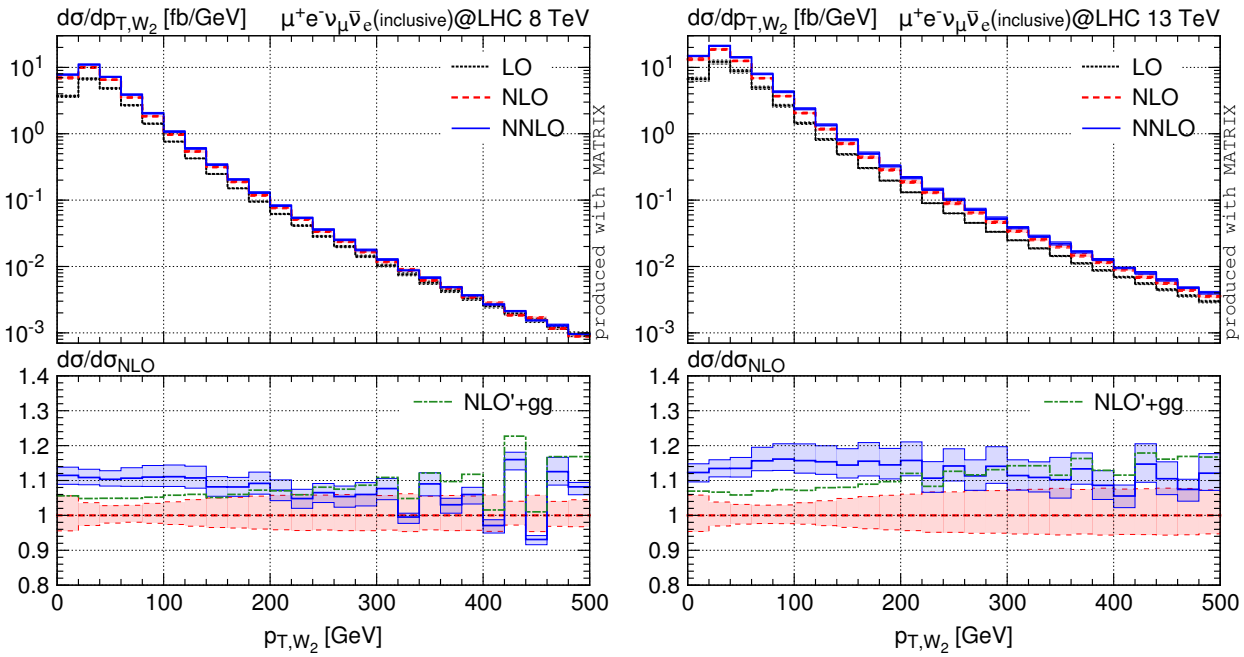

(a) (b)

Figure 7: Distribution in the transverse momentum of the softer reconstructed W boson. No acceptance cuts are applied. Absolute predictions and relative corrections as in Figure 4.

and subleading W boson, the NNLO corrections tend to exceed the NLO scale band at moderate transverse-momentum values.

For all distributions discussed so far, we find qualitatively the same effects at 8 and 13 TeV, essentially only differing by the larger overall size of the NNLO corrections at the higher collider energy. Contributing only about one third of the total NNLO correction, the NLO′+gg approximation does not provide a reliable description of the full NNLO result. Moreover, in general the loop-induced gluon–gluon channel alone cannot reproduce the correct shapes of the full NNLO correction.

3.3 Analysis of $\mu^+e^-\nu_\mu\bar{\nu}_e$ production with W^+W^- selection cuts

In this Section we investigate the behaviour of radiative corrections in presence of acceptance cuts used in W^+W^- measurements. The full set of cuts is summarized in Table 1 and is inspired by the W^+W^- analysis of Ref. [6][‖]. Besides various restrictions on the leptonic degrees of freedom and the missing transverse momentum, this analysis implements a jet veto.

Predictions for fiducial cross sections at different perturbative orders are reported in Table 3. As a result of fiducial cuts, in particular the jet veto, radiative corrections behave very differently as compared to the inclusive case. The NLO corrections with respect to LO amount to only about +4% (+1%) at 8 (13) TeV. Neglecting the +2% (+3%) shift due to the PDFs, the NNLO corrections amount to +5% (+7%). Their positive impact is, however, entirely due to the loop-induced gluon-fusion contribution, which is not affected by the jet veto. In fact, comparing the NNLO and NLO′+gg predictions we see that the genuine $\mathcal{O}(\alpha_S^2)$ corrections are negative and amount to roughly −1% (−2%).

The reduction of the impact of radiative corrections when a jet veto is applied is a well-known feature in perturbative QCD calculations [111]. A stringent veto on the radiation recoiling against the W^+W^- system tends to unbalance the cancellation between positive real and negative virtual contributions, possibly leading to large logarithmic terms. The resummation of such logarithms has been the subject of intense theoretical studies, especially in the important case of Higgs-boson production [112–114], and it has been recently addressed also for W^+W^- production [51, 52]. In the case at hand, the moderate size of radiative effects beyond NLO suggests that, similarly as for Higgs production, fixed-order NNLO predictions should provide a fairly reliable description of jet-vetoed fiducial cross sections and distributions.

The reduced impact of radiative effects in the presence of a jet veto is often accompanied by a reduction of scale uncertainties in fixed-order perturbative calculations. Comparing the results in Table 3 with those in Table 2 we indeed see that the size of the NNLO scale uncertainty is reduced when cuts, particularly the jet veto, are applied. Such a small scale dependence should be interpreted with caution as it tends to underestimate the true uncertainty due to missing higher-order perturbative contributions.

The effect of radiative corrections on the efficiency of W^+W^- fiducial cuts,

$$\epsilon = \sigma_{\text{fiducial}}/\sigma_{\text{inclusive}}\,, \tag{4}$$

[‖]We do not apply any lepton-isolation criteria with respect to hadronic activity.

	$\sigma_{\text{fiducial}}(W^+W^-\text{-cuts})$ [fb]		$\sigma/\sigma_{\text{NLO}} - 1$	
$\sqrt{s}$	8 TeV	13 TeV	8 TeV	13 TeV
LO	$147.23\ (2)\,^{+3.4\%}_{-4.4\%}$	$233.04(2)\,^{+6.6\%}_{-7.6\%}$	-3.8%	$-\ 1.3\%$
NLO	$153.07\ (2)\,^{+1.9\%}_{-1.6\%}$	$236.19(2)\,^{+2.8\%}_{-2.4\%}$	0	0
NLO′	$156.71\ (3)\,^{+1.8\%}_{-1.4\%}$	$243.82(4)\,^{+2.6\%}_{-2.2\%}$	$+2.4\%$	$+\ 3.2\%$
NLO′+gg	$166.41\ (3)\,^{+1.3\%}_{-1.3\%}$	$267.31(4)\,^{+1.5\%}_{-2.1\%}$	$+8.7\%$	$+13.2\%$
NNLO	$164.16(13)\,^{+1.3\%}_{-0.8\%}$	$261.5(2)\ \ ^{+1.9\%}_{-1.2\%}$	$+7.2\%$	$+10.7\%$

Table 3: Cross sections with W^+W^- fiducial cuts at different perturbative orders and relative differences with respect to NLO. Scale uncertainties and errors as in Table 2.

	$\epsilon = \sigma_{\text{fiducial}}(W^+W^-\text{-cuts})/\sigma_{\text{inclusive}}$		$\epsilon/\epsilon_{\text{NLO}} - 1$	
$\sqrt{s}$	8 TeV	13 TeV	8 TeV	13 TeV
LO	$0.34608(7)^{+0.6\%}_{-0.7\%}$	$0.29915(6)^{+0.8\%}_{-1.0\%}$	$+41.0\%$	$+52.6\%$
NLO	$0.24552(5)^{+4.4\%}_{-4.7\%}$	$0.19599(4)^{+4.4\%}_{-4.7\%}$	0	0
NLO′+gg	$0.25374(7)^{+3.5\%}_{-3.7\%}$	$0.20773(5)^{+3.2\%}_{-3.1\%}$	$+\ 3.3\%$	$+\ 6.0\%$
NNLO	$0.2378(4)\ ^{+1.3\%}_{-0.9\%}$	$0.1907(3)\ ^{+1.2\%}_{-0.9\%}$	$-\ 3.2\%$	$-\ 2.7\%$

Table 4: Efficiency of W^+W^- acceptance cuts at different perturbative orders and relative differences with respect to NLO. Scale uncertainties and errors as in Table 2.

is illustrated in Table 4, where numerator and denominator are evaluated at the same perturbative order and both with $\mu_R = \mu_F = m_W$. Due to the negative impact of the newly computed NNLO corrections on the fiducial cross section (see Table 3) and their positive impact on the inclusive cross section (see Table 2), the NNLO corrections on the cut efficiency are quite significant. In particular, at $\sqrt{s} = 8\,(13)$ TeV the full NNLO prediction lies about 6% (9%) below the NLO′+gg result. The uncertainties quoted in Table 4 are obtained by varying μ_R and μ_F in a fully correlated way in the numerator and denominator of Eq. (4). Clearly, there is a large correlation at LO, which results in a particularly small uncertainty. At NNLO the uncertainties are comparable to those of the fiducial cross sections.

As discussed in Section 2.1, our default 4FS predictions are compared to an alternative top-subtracted computation in the 5FS, in order to assess the uncertainty related to the prescription for the subtraction of the top contamination. Without top subtraction we obtain $\sigma_{\text{NLO}} = 165.7(3)$ fb and $\sigma_{\text{NNLO}} = 181.9(4)$ fb at $\sqrt{s} = 8$ TeV in the 5FS. Due to the jet veto, these fiducial cross sections feature a moderate top contamination of about 8% at NLO and 12% at NNLO. Removing the top contributions, we find $\sigma_{\text{NLO}} = 153.4(4)$ fb and $\sigma_{\text{NNLO}} = 162.5(3)$ fb, which agree with the 4FS results within 1%. At $\sqrt{s} = 13$ TeV, the top contamination in the 5FS is somewhat larger and amounts to 12% (17%) at NLO (NNLO). The top-subtracted fiducial cross sections,

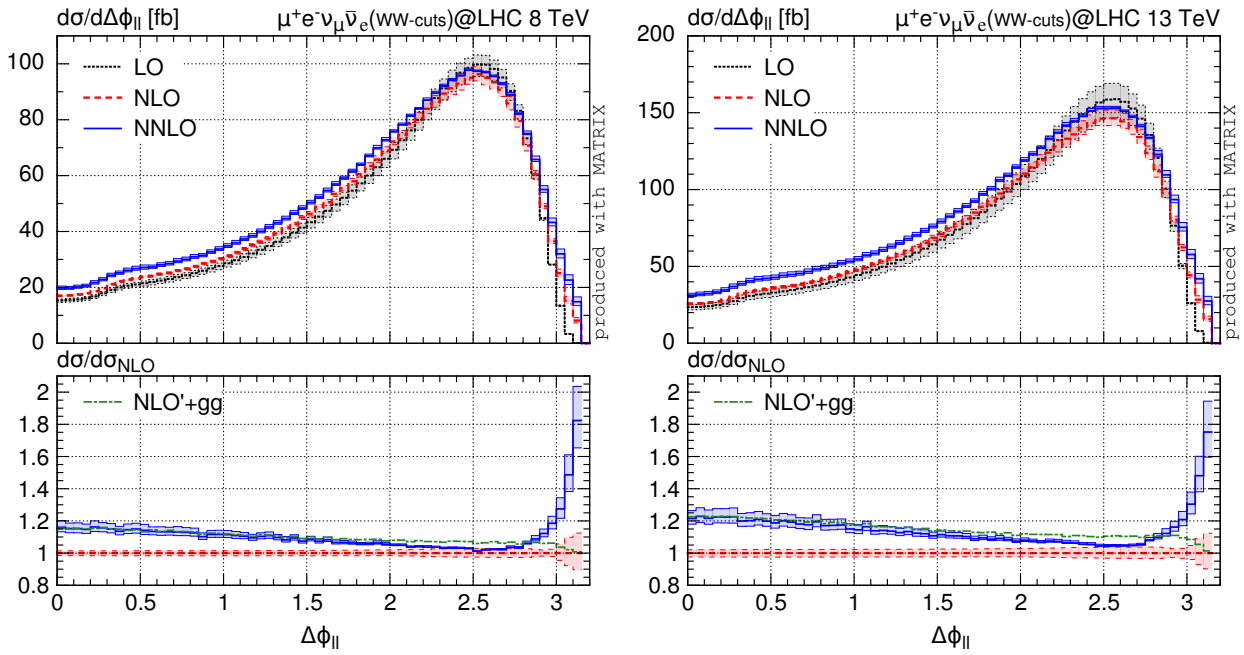

(a) (b)

Figure 8: Distribution in the azimuthal separation of the charged leptons. W^+W^- cuts are applied. Absolute predictions and relative corrections as in Figure 4.

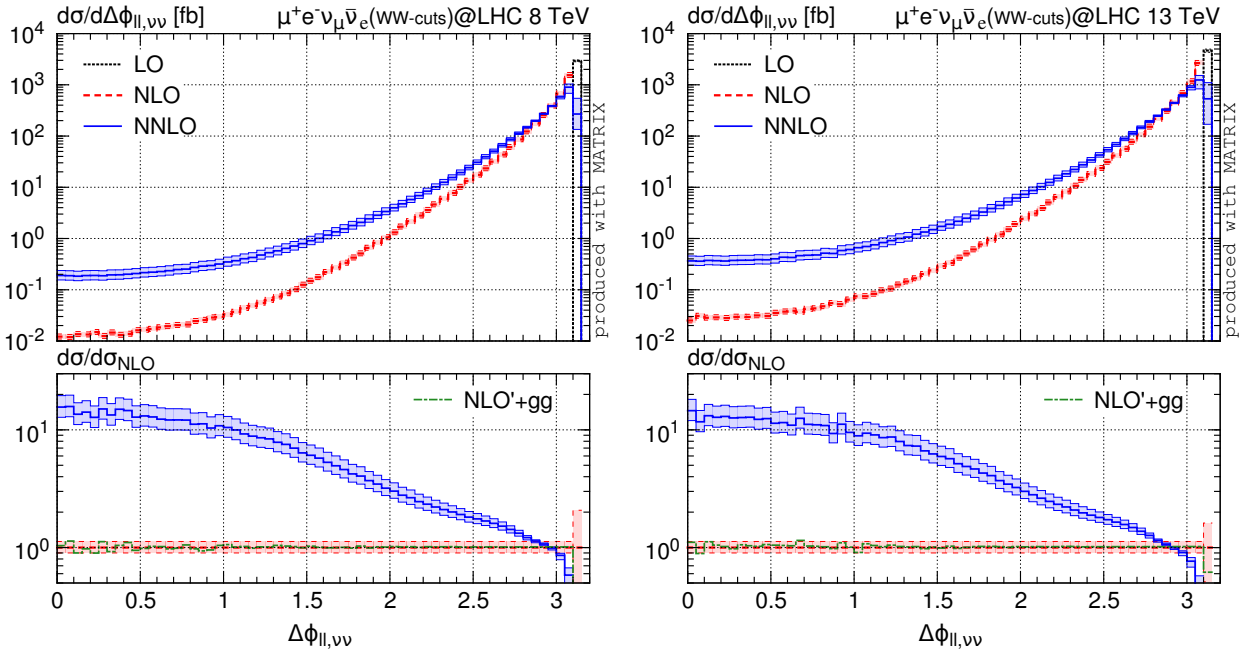

(a) (b)

Figure 9: Distribution in the azimuthal separation between the transverse momentum of the dilepton system and the missing transverse momentum. W^+W^- cuts are applied. Absolute predictions and relative corrections as in Figure 4.

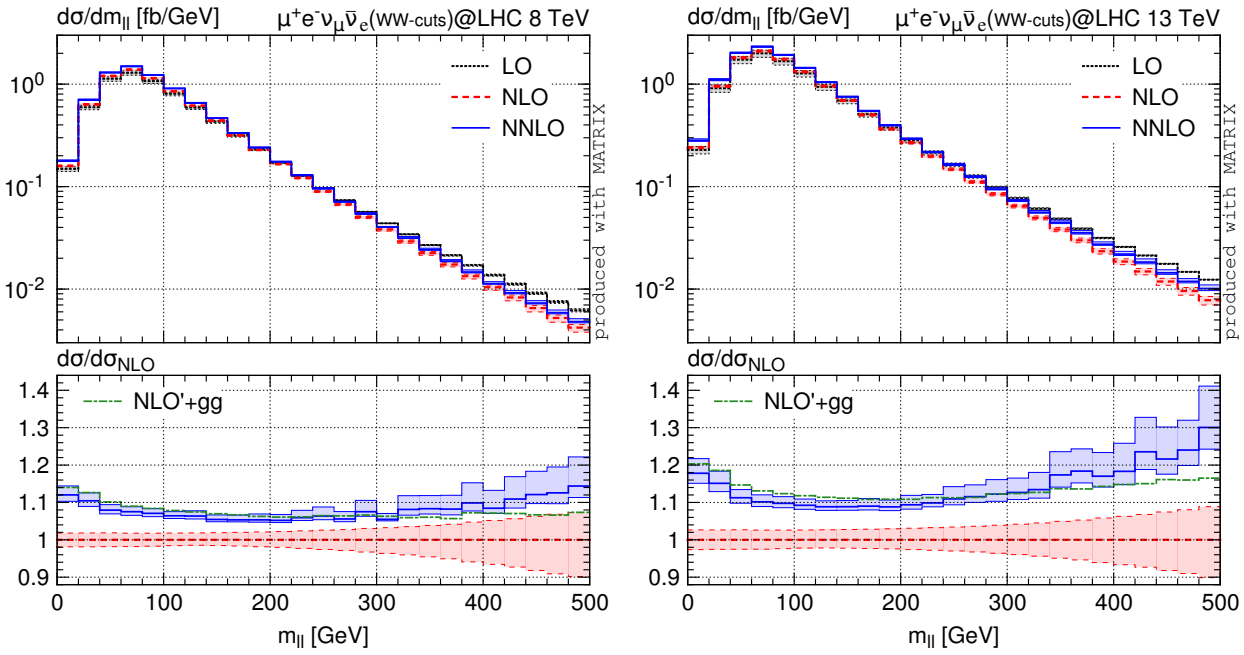

(a) (b)

Figure 10: Distribution in the dilepton invariant mass. W^+W^- cuts are applied. Absolute predictions and relative corrections as in Figure 4.

$\sigma_{\rm NLO} = 238.3(6)\,{\rm fb}$ and $\sigma_{\rm NNLO} = 265(2)\,{\rm fb}$, on the other hand, are again in agreement with the 4FS results at the $1\% - 2\%$ level.

Differential distributions in presence of W^+W^- fiducial cuts are presented in Figures 8–15. We first consider, in Figure 8, the distribution in the azimuthal separation of the charged leptons, $\Delta\phi_{ll}$. The NLO′+gg approximation is in good agreement with full NNLO result at small $\Delta\phi_{ll}$, but in the peak region the difference exceeds 5%, and the NLO′+gg result lies outside the NNLO uncertainty band. The difference significantly increases in the large $\Delta\phi_{ll}$ region, where the cross section is strongly suppressed though. The uncertainty bands of the NLO and NNLO predictions do not overlap. This feature is common to all distributions that are considered in the following. It is primarily caused by the loop-induced gg contribution, which enters only at NNLO and is not accounted for by the NLO scale variations. Ignoring the gluon-induced component, we observe a good perturbative convergence, apart from some peculiar phase-space corners.

In Figure 9 we study the cross section as a function of the azimuthal separation $\Delta\phi_{ll,\nu\nu}$ between the transverse momentum of the dilepton pair ($\mathbf{p_{T,ll}}$) and the missing transverse momentum ($\mathbf{p_T^{miss}}$). Since $\Delta\phi_{ll,\nu\nu} = \pi$ at LO, the (N)NLO calculation is only (N)LO accurate at $\Delta\phi_{ll,\nu\nu} < \pi$. The NNLO corrections have a dramatic impact on the shape of the distribution: The $\sigma_{\rm NNLO}/\sigma_{\rm NLO}$ K-factor grows with decreasing $\Delta\phi_{ll,\nu\nu}$ and reaches up to $\mathcal{O}(10)$ in the region $\Delta\phi_{ll,\nu\nu} \lesssim 1$, where the cross section is suppressed by more than three orders of magnitude. This huge effect results from the interplay of the jet veto with the cuts on the p_T's of the individual leptons and on $p_T^{\rm miss}$. At small $\Delta\phi_{ll,\nu\nu}$ the transverse momenta $\mathbf{p_{T,ll}}$ and $\mathbf{p_T^{miss}}$ must be balanced by recoiling QCD partons. However, at NLO the emitted parton can deliver a sizeable recoil only in the region

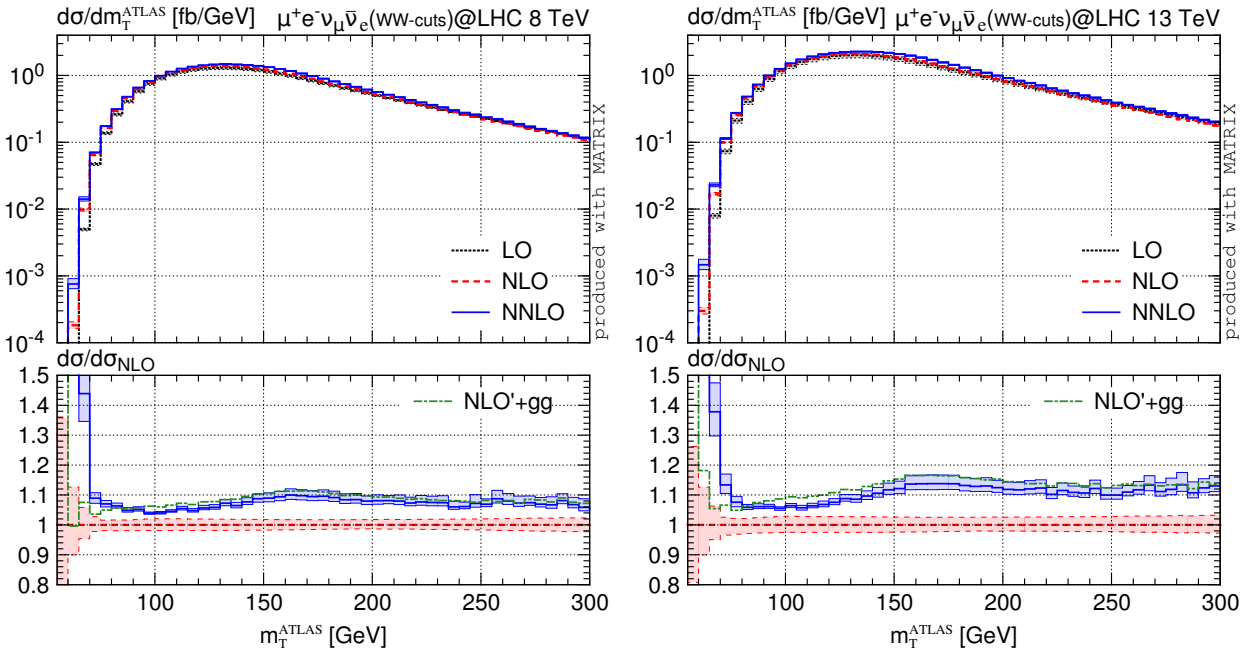

(a) (b)

Figure 11: Distribution in the W^+W^- transverse mass. W^+W^- cuts are applied. Absolute predictions and relative corrections as in Figure 4.

that is not subject to the jet veto, i.e. in the strongly suppressed rapidity range $|y_j| > 4.5$. At NNLO, the presence of a second parton relaxes this restriction to some extent, thereby reducing the suppression by about one order of magnitude. The loop-induced gg contribution does not involve any QCD radiation and contributes only at $\Delta\phi_{ll,\nu\nu} = \pi$. As a consequence, the NLO and NLO$'$+gg predictions at $\Delta\phi_{ll,\nu\nu} < \pi$ are almost identical, apart from minor differences due to the PDFs.

The invariant-mass distribution of the dilepton pair is presented in Figure 10. On the one hand, if one takes into account NNLO scale variations, the NLO$'$+gg result is by and large consistent with the NNLO prediction. On the other hand, the shapes of the NLO$'$+gg and NNLO distributions feature non-negligible differences, which range from +5% at low masses to −5% in the high-mass tail. Nevertheless, NLO$'$+gg provides a reasonable approximation of the full NNLO result, in particular regarding the normalization.

The distribution in the W^+W^- transverse mass,

$$m_T^{\rm ATLAS} = \sqrt{\left(E_{T,l_1} + E_{T,l_2} + p_T^{\rm miss}\right)^2 - \left(\mathbf{p}_{T,l_1} + \mathbf{p}_{T,l_2} + p_T^{\rm miss}\right)^2}\,, \tag{5}$$

is displayed in Figure 11. Also in this case, apart from the strongly suppressed region of small $m_T^{\rm ATLAS}$, the NLO$'$+gg approximation is in quite good agreement with the full NNLO prediction.

In Figures 12 and 13 we show results for the p_T distributions of the leading and subleading lepton, respectively. In both cases the impact of NNLO corrections grows with p_T. This is driven by the gluon-induced contribution, which overshoots the complete NNLO result in the small-p_T

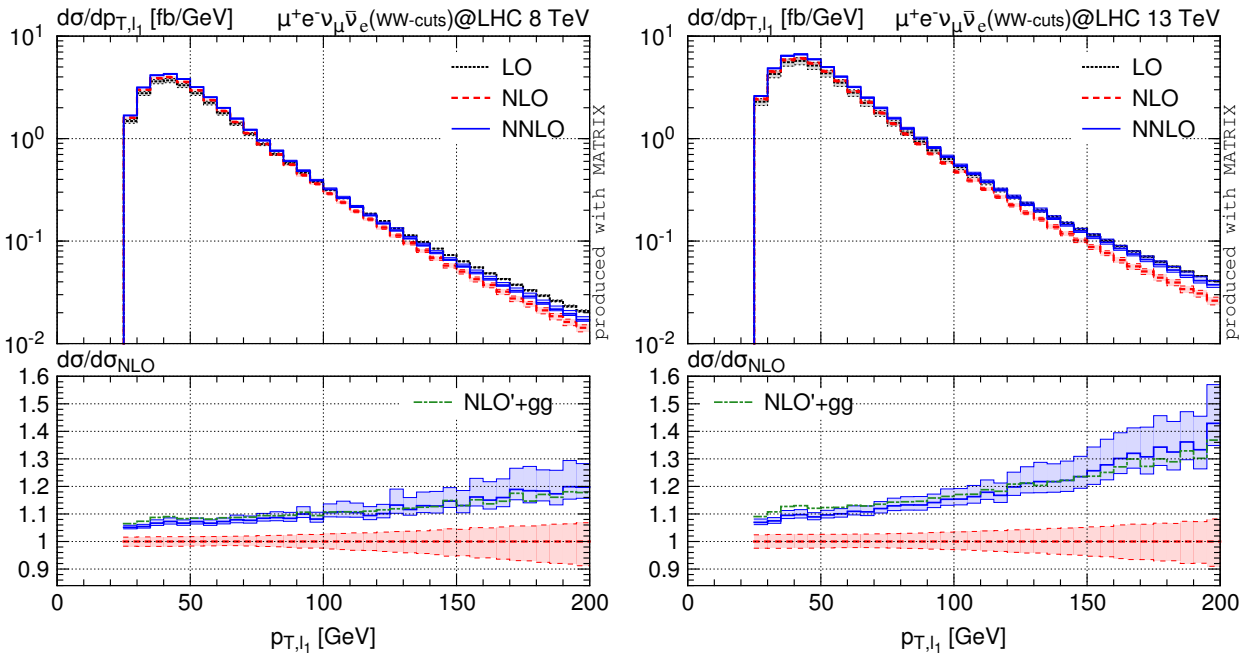

(a) (b)

Figure 12: Distribution in the p_T of the leading lepton. W^+W^- cuts are applied. Absolute predictions and relative corrections as in Figure 4.

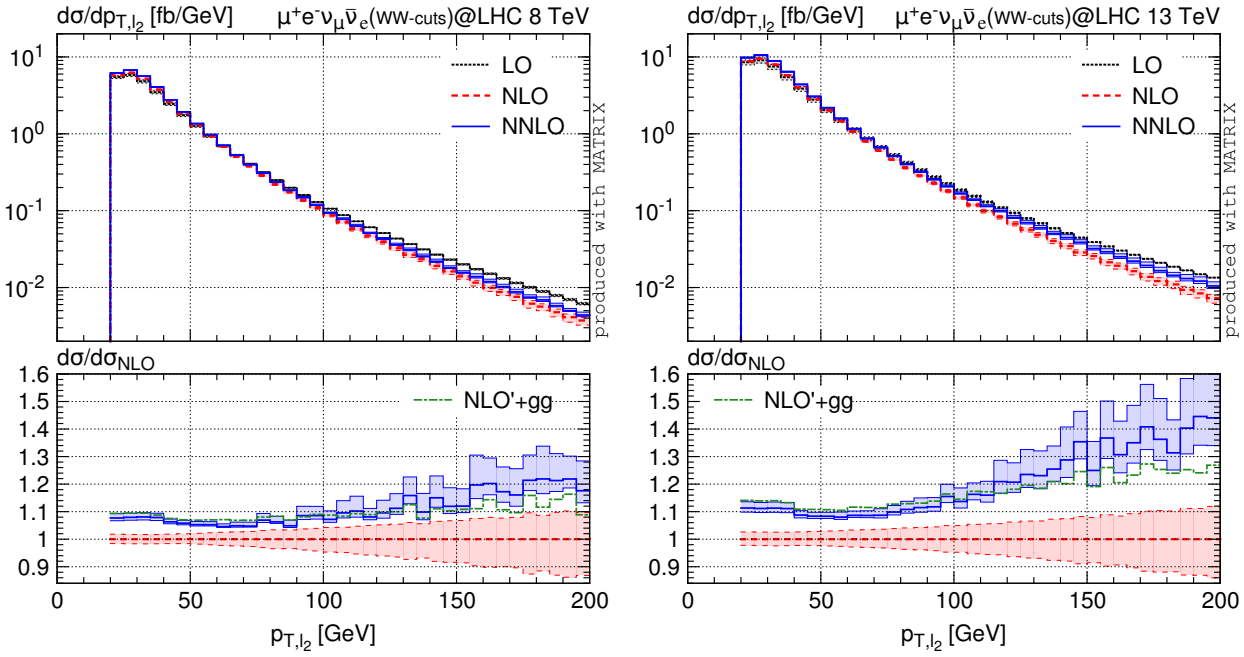

(a) (b)

Figure 13: Distribution in the p_T of the subleading lepton. W^+W^- cuts are applied. Absolute predictions and relative corrections as in Figure 4.

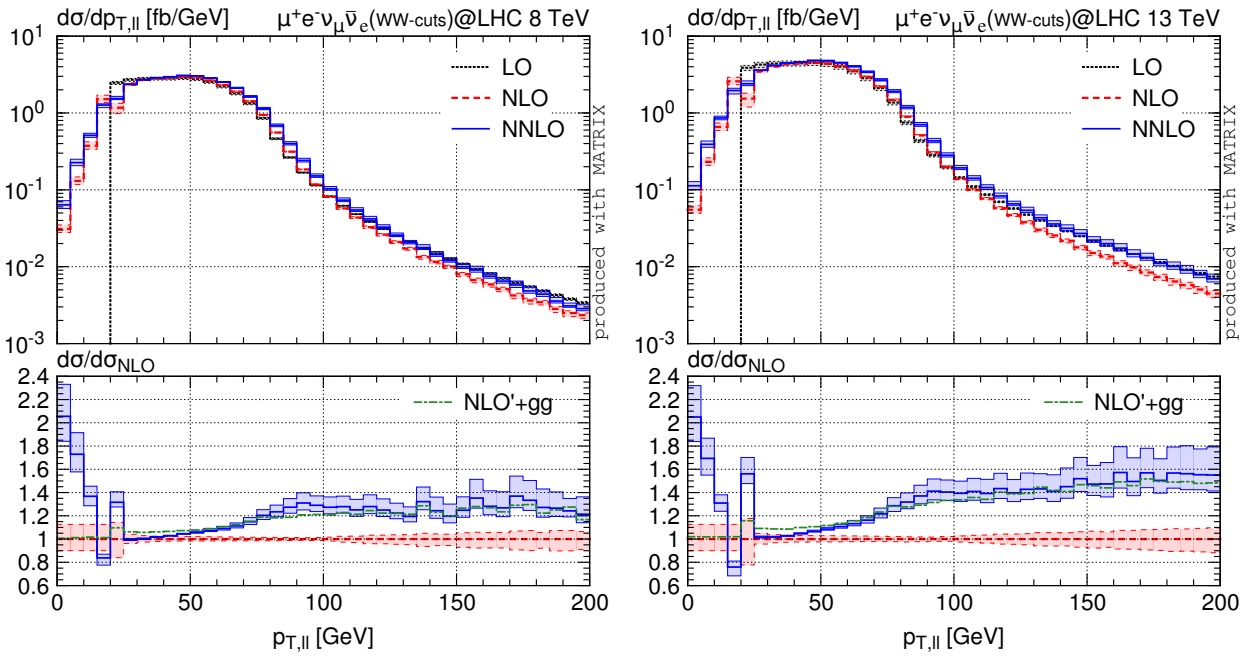

(a) (b)

Figure 14: Distribution in the p_T of the dilepton system. W^+W^- cuts are applied. Absolute predictions and relative corrections as in Figure 4.

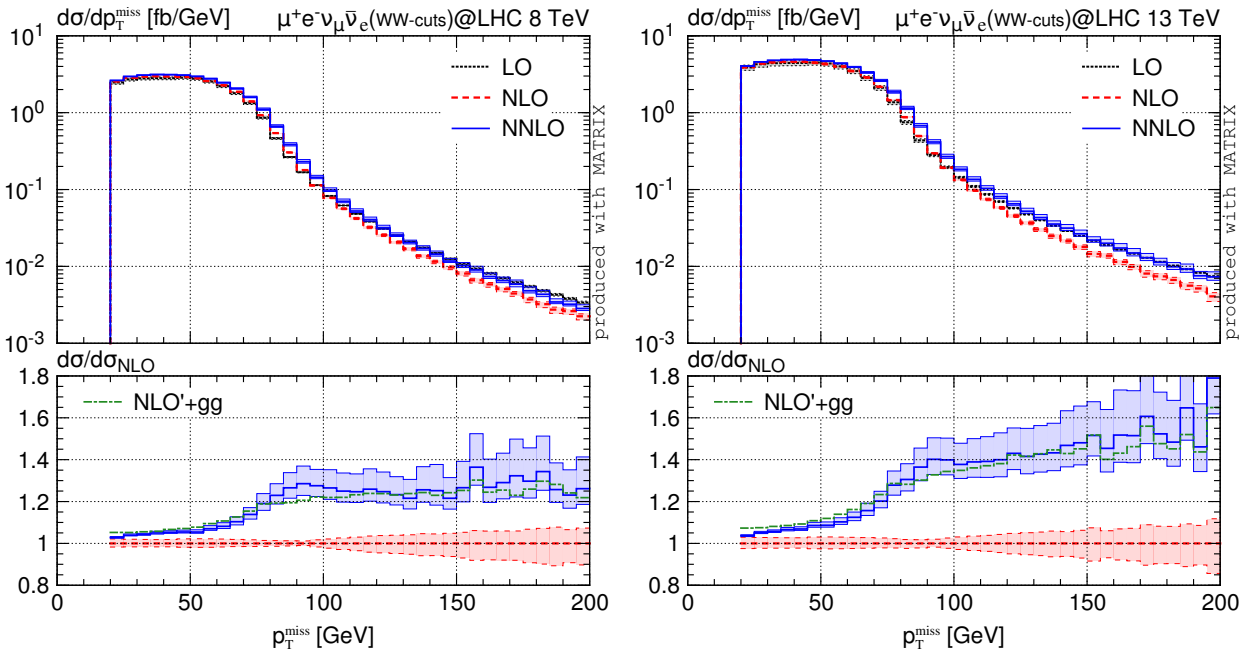

(a) (b)

Figure 15: Distribution in the missing transverse momentum. W^+W^- cuts are applied. Absolute predictions and relative corrections as in Figure 4.

region and behaves in the opposite way as p_T becomes large. In the case of the subleading lepton, the genuine NNLO corrections are as large as $\mathcal{O}(10\%)$ around $p_{T,l_2} = 200\,\text{GeV}$. Overall, there is a visible difference in shape between NLO′+gg and NNLO for both the leading and subleading lepton transverse-momentum distributions.

The p_T distribution of the dilepton pair is displayed in Figure 14. This observable has a kinematical boundary at LO, where the requirement $p_T^{\text{miss}} > 20$ GeV implies that $p_{T,ll} > 20$ GeV. The region $p_{T,ll} < 20$ GeV starts to be populated at NLO, but each perturbative higher-order contribution (beyond LO) produces integrable logarithmic singularities leading to perturbative instabilities at the boundary [115]. This becomes particularly evident in the $d\sigma_{\text{NNLO}}/d\sigma_{\text{NLO}}$ ratio. The loop-induced gg contribution, having Born-like kinematics, does not contribute to the region $p_{T,ll} < 20$ GeV. In contrast, NNLO corrections are huge, and the formal accuracy of NNLO predictions is only NLO in that region. In the region of high $p_{T,ll}$ we observe significant NNLO corrections, and the NLO′+gg approximation works rather well. Similar features are observed in the p_T^{miss} distribution, displayed in Figure 15, but without the perturbative instability at $p_T^{\text{miss}} = 20\,\text{GeV}$, as the cut on p_T^{miss} is explicit.

In general, radiative corrections behave in a rather similar way at $\sqrt{s} = 8\,\text{TeV}$ and $\sqrt{s} = 13\,\text{TeV}$ in presence of W^+W^- cuts. Comparing the NLO′+gg approximation with the full NNLO prediction, we find that the overall normalization is typically reproduced quite well, while genuine NNLO corrections can lead to significant shape differences of up to 10%. It does not come as a surprise that in kinematic regions that imply the presence of QCD radiation, loop-induced gg contributions cannot provide a reasonable approximation of the full NNLO correction.

3.4 Analysis of $\mu^+e^-\nu_\mu\bar{\nu}_e$ production with Higgs selection cuts

In this Section we repeat our study of radiative corrections in presence of cuts that are designed for $H \to W^+W^-$ studies at the LHC. In this case, W^+W^- production plays the role of irreducible background, and more stringent cuts are applied in order to minimize its impact on the $H \to W^+W^-$ signal. The precise list of cuts is specified in Table 1 and corresponds to the $H \to W^+W^-$ analysis of Ref. [12]**. This selection implements a series of cuts similar to the ones used in W^+W^- signal measurements, including a jet veto. The suppression of on-shell W^+W^- production is achieved through additional restrictions on $p_{T,ll}$, m_{ll}, $\Delta\phi_{ll}$ and $\Delta\phi_{ll,\nu\nu}$.

In Table 5 we report predictions for fiducial cross sections at different perturbative orders. The corresponding acceptance efficiencies, computed as in Section 3.3, are presented in Table 6. It turns out that Higgs cuts suppress the impact of QCD radiative effects in a similar way as W^+W^- cuts. At 8 (13) TeV the NLO and NNLO corrections amount to +5% (+3%) and to +9% (+13%), respectively. The latter consist of a positive +3% shift due to NNLO PDFs, a sizeable loop-induced gg component of +9% (+13%), and a rather small genuine $\mathcal{O}(\alpha_S^2)$ contribution of −2% (−4%).

We compare the 4FS predictions against the top-subtracted calculation in the 5FS: At $\sqrt{s} = 8\,(13)\,\text{TeV}$ the latter yields $\sigma_{\text{NLO}} = 48.7\,(3)\,\text{fb}$ ($\sigma_{\text{NLO}} = 73.4\,(2)\,\text{fb}$) and $\sigma_{\text{NNLO}} = 53.0\,(5)\,\text{fb}$ ($\sigma_{\text{NNLO}} = 83.1\,(5)\,\text{fb}$), which corresponds to a $1\% - 2\%$ agreement with the 4FS results. The size of

**In our analysis, we require $|y_\mu| < 2.4$ as for W^+W^- signal cuts, in contrast to $|y_\mu| < 2.5$ in the ATLAS analysis. Moreover, we do not apply any lepton-isolation criteria with respect to hadronic activity.

	σ_{fiducial}(H−cuts) [fb]		$\sigma/\sigma_{\text{NLO}} - 1$	
$\sqrt{s}$	8 TeV	13 TeV	8 TeV	13 TeV
LO	$45.923(4)\,^{+4.0\%}_{-5.0\%}$	$71.164\ (7)\,^{+7.2\%}_{-8.2\%}$	− 4.4%	− 2.6%
NLO	$48.045(5)\,^{+1.9\%}_{-1.7\%}$	$73.085\ (6)\,^{+2.7\%}_{-2.4\%}$	0	0
NLO′	$49.318(7)\,^{+1.7\%}_{-1.6\%}$	$75.578(11)\,^{+2.5\%}_{-2.2\%}$	+ 2.7%	+ 3.4%
NLO′+gg	$53.496(8)\,^{+2.0\%}_{-1.5\%}$	$85.231(12)\,^{+2.5\%}_{-2.5\%}$	+11.3%	+16.6%
NNLO	$52.30(4)\ \,^{+1.6\%}_{-1.0\%}$	$82.32(12)\ \,^{+2.4\%}_{-2.6\%}$	+ 8.9%	+12.6%

Table 5: Cross sections with Higgs fiducial cuts at different perturbative orders and relative differences with respect to NLO. Scale uncertainties and errors as in Table 2.

	$\epsilon = \sigma_{\text{fiducial}}$(H−cuts)$/\sigma_{\text{inclusive}}$		$\epsilon/\epsilon_{\text{NLO}} - 1$	
$\sqrt{s}$	8 TeV	13 TeV	8 TeV	13 TeV
LO	$0.10795\ (2)^{+1.2\%}_{-1.4\%}$	$0.09135\ (2)^{+1.5\%}_{-1.7\%}$	+40.1%	+50.6%
NLO	$0.07706\ (2)^{+4.3\%}_{-4.6\%}$	$0.06065\ (1)^{+4.3\%}_{-4.5\%}$	0	0
NLO′+gg	$0.08157\ (2)^{+3.1\%}_{-3.1\%}$	$0.06623\ (2)^{+2.7\%}_{-2.5\%}$	+ 5.9%	+ 9.2%
NNLO	$0.07575(11)^{+1.2\%}_{-0.8\%}$	$0.06005(14)^{+1.1\%}_{-0.9\%}$	− 1.7%	− 1.0%

Table 6: Efficiency of Higgs acceptance cuts at different perturbative orders and relative differences with respect to NLO. Scale uncertainties and errors as in Table 2.

the subtracted top contamination in the 5FS is slightly smaller than what was found for W^+W^- cuts. It amounts to 5% (9%) at NLO and 6% (11%) at NNLO.

Similarly to the case of W^+W^- cuts, genuine $\mathcal{O}(\alpha_S^2)$ corrections have a significant impact on the acceptance efficiency: At $\sqrt{s} = 8\,(13)$ TeV the NNLO prediction lies roughly 8% (10%) below the NLO′+gg result, which exceeds the respective scale uncertainties. While the relative size of higher-order effects on the Higgs-cut efficiency is almost identical to the one found for W^+W^- selection cuts, the absolute size of the acceptance efficiencies is much smaller. In the case of Higgs cuts it is almost a factor of three lower, primarily due to the stringent cut on the invariant mass of the dilepton system.

Differential distributions with Higgs cuts applied are presented in Figures 16–23. In general, they behave in a similar way as for the case of W^+W^- cuts discussed in Section 3.3. However, a few observables are quite sensitive to the additional cuts that are applied in the Higgs analysis. Most notably, the distribution in the azimuthal separation of the charged leptons in Figure 16 exhibits a completely different shape as compared to Figure 8. In particular, it features an approximate plateau in the region $0.4 \leq \Delta\phi_{ll} \leq 1.2$. The NNLO corrections with respect to the NLO distribution at $\sqrt{s} = 8\,(13)$ TeV range from about +13% (+18%) at small $\Delta\phi_{ll}$ to roughly

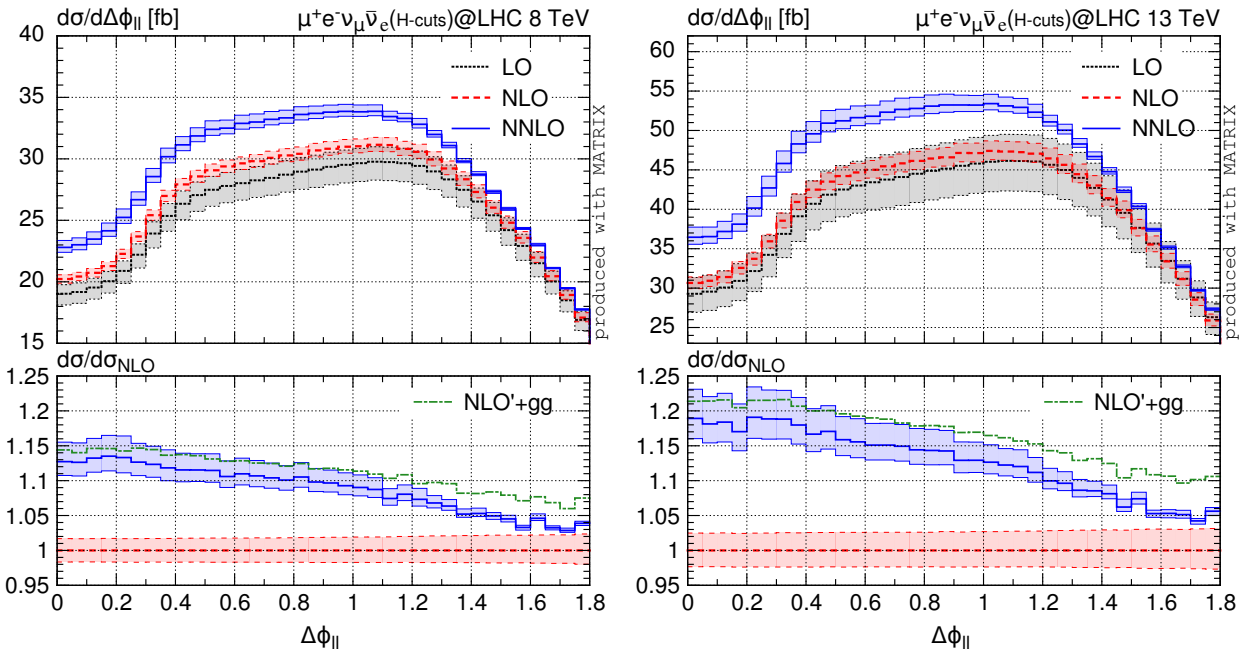

(a) (b)

Figure 16: Distribution in the azimuthal separation of the charged leptons. Higgs cuts are applied. Absolute predictions and relative corrections as in Figure 4.

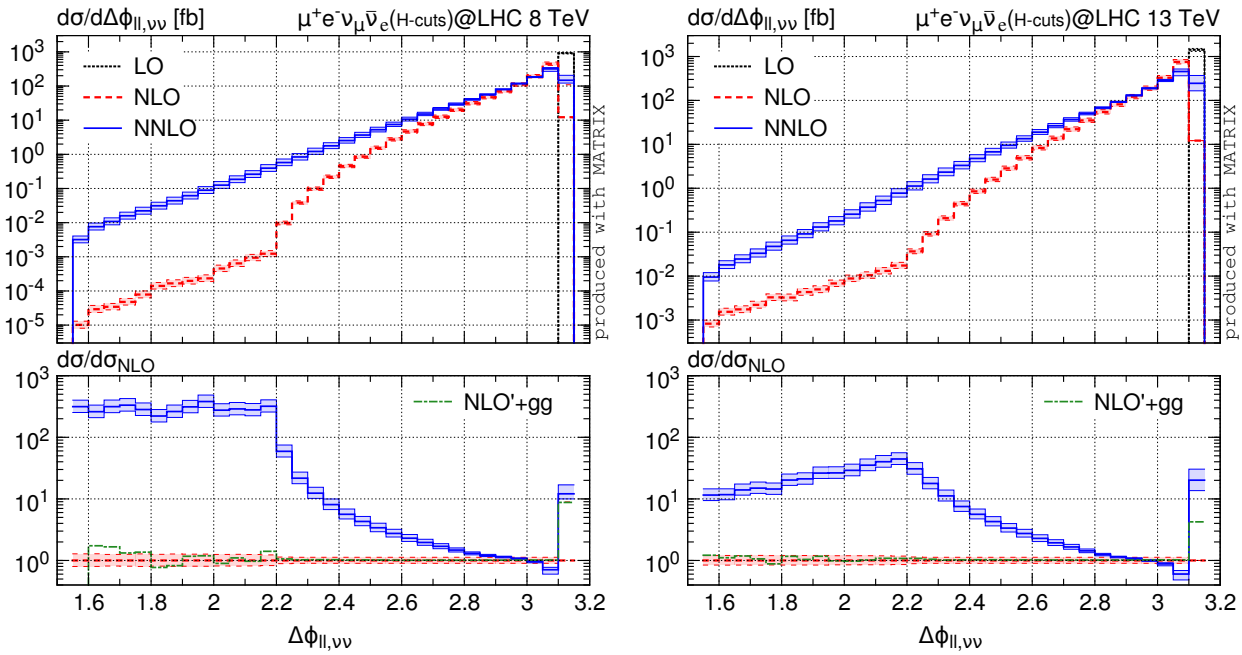

(a) (b)

Figure 17: Distribution in the azimuthal separation between the transverse momentum of the dilepton system and the missing transverse momentum. Higgs cuts are applied. Absolute predictions and relative corrections as in Figure 4.

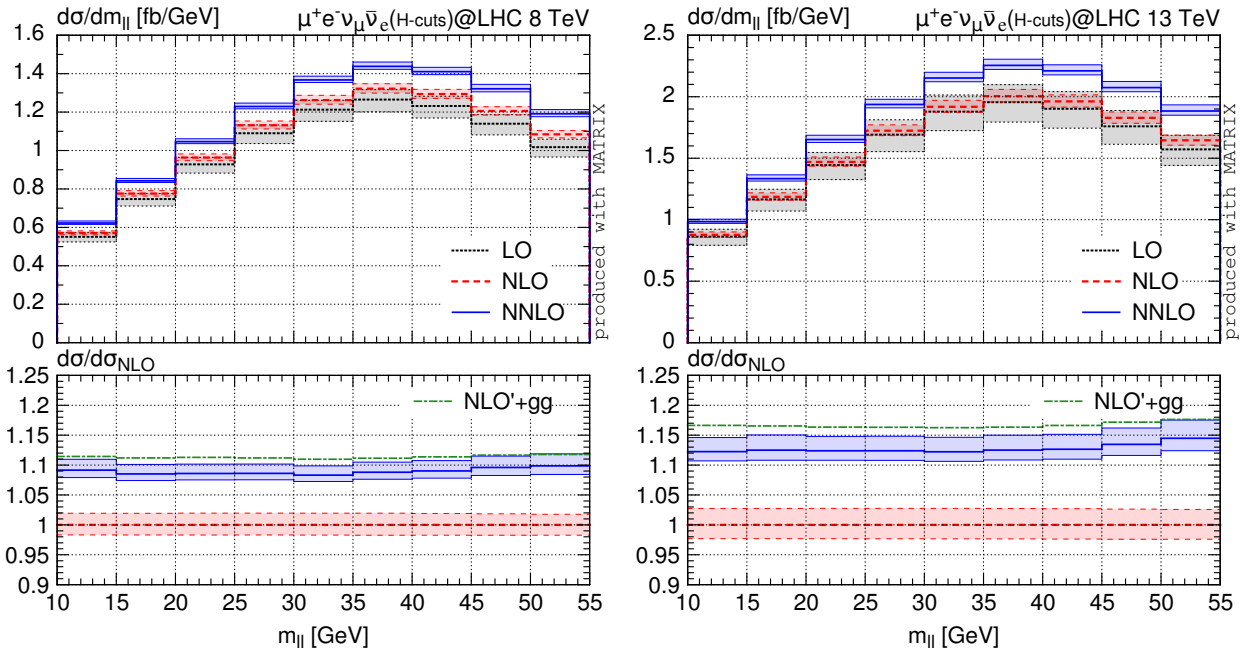

(a) (b)

Figure 18: Distribution in the dilepton invariant mass. Higgs cuts are applied. Absolute predictions and relative corrections as in Figure 4.

+2% (+5%) at separations close to the fiducial cut. The loop-induced gg component provides a good approximation of the complete NNLO result for small separations, but in the large $\Delta\phi_{ll}$ region it overshoots the complete NNLO result by about 5% (7%).

In the $\Delta\phi_{ll,\nu\nu}$ distribution, displayed in Figure 17, we observe that, similarly to the case of W^+W^- cuts (see Figure 9), also Higgs cuts lead to huge NNLO corrections at small $\Delta\phi_{ll,\nu\nu}$. As discussed in Section 3.3, this behaviour is due to the fact that at small $\Delta\phi_{ll,\nu\nu}$ the leptonic and p_T^{miss} cuts require the presence of a sizeable QCD recoil, which is, however, strongly suppressed by the jet veto at NLO. In the Higgs analysis, this suppression mechanism becomes even more powerful due to the additional cut $p_{T,ll} > 30\,\text{GeV}$, which forbids the two leptons to recoil against each other. This leads to the kink at $\Delta\phi_{ll,\nu\nu} = 2.2$ in the NLO distribution and to the explosion of NNLO corrections below and slightly above this threshold.

The invariant mass of the dilepton system, shown in Figure 18, is restricted to the region $10\,\text{GeV} \leq m_{ll} \leq 55\,\text{GeV}$. The peak of the distribution is around $m_{ll} = 38\,\text{GeV}$, and the $\sigma_{\text{NNLO}}/\sigma_{\text{NLO}}$ K-factor is essentially flat. Also the NLO′+gg curve has a very similar shape so that the radiative corrections precisely match those on the fiducial rates.

The distribution in m_T^{ATLAS} is presented in Figure 19. As compared to the W^+W^- analysis (see Figure 11), we observe that the tail of the distribution drops significantly faster when Higgs cuts are applied. Moreover, in the high-m_T^{ATLAS} region the size of the loop-induced gg corrections relative to NLO and, hence, the size of the full NNLO correction, is much larger than in the W^+W^- analysis. The NNLO corrections amount up to about 40% (60%) of the NLO cross section

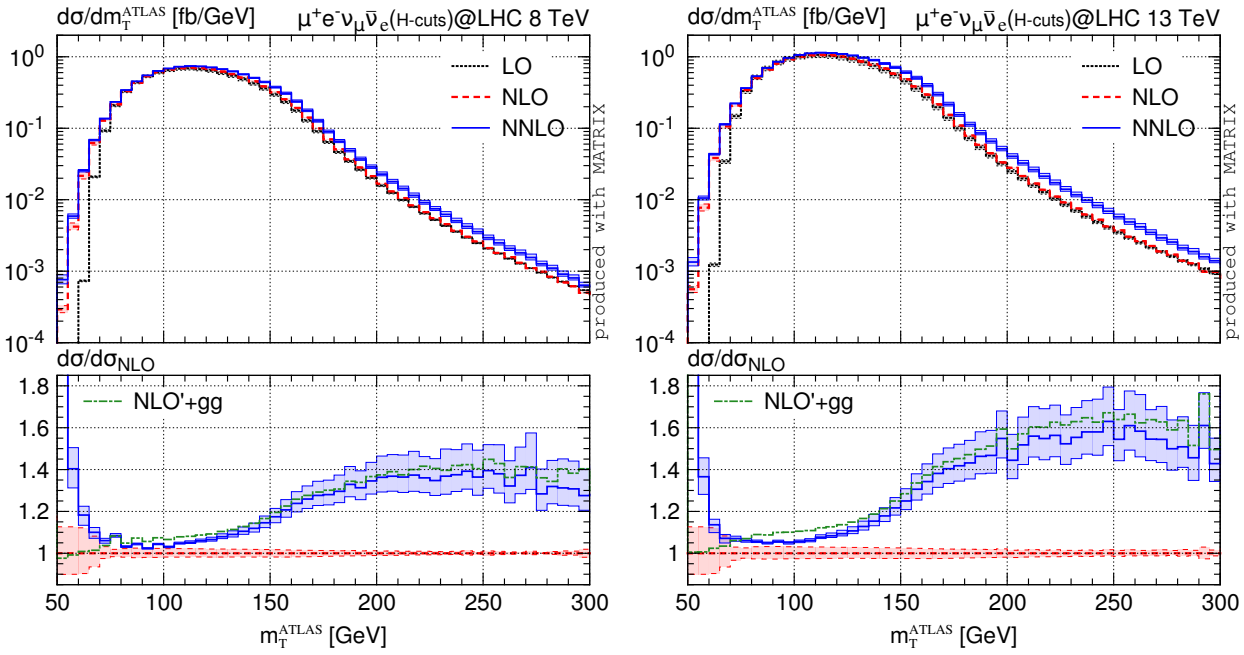

(a) (b)

Figure 19: Distribution in the W^+W^- transverse mass. Higgs cuts are applied. Absolute predictions and relative corrections as in Figure 4.

at $\sqrt{s} = 8\,(13)$ TeV, while they hardly exceed 15% when W^+W^- cuts are applied.

The distributions in the lepton p_T's, depicted in Figures 20 and 21, behave in a similar way as in Figures 12 and 13, apart from a steeper drop-off in the tail and slightly larger corrections.

For the distributions in the p_T of the dilepton pair (see Figure 22) and in $p_T^{\rm miss}$ (see Figure 23), we also find a similar behaviour as in the case where W^+W^- cuts are applied. We note, however, that the perturbative instability observed in the $p_{T,ll}$ distribution with W^+W^- cuts (see Figure 14) is removed by the explicit cut $p_{T,ll} > 30\,\text{GeV}$ in the Higgs analysis. Accordingly, the $p_{T,ll}$ cut implicitly vetoes events with $p_T^{\rm miss} < 30\,\text{GeV}$ at Born level, which leads to a perturbative instability in the $p_T^{\rm miss}$ distribution, particularly visible in the $\sigma_{\rm NNLO}/\sigma_{\rm NLO}$ ratio. In fact, it is evident from Figure 23 that the phase-space region $p_T^{\rm miss} < 30\,\text{GeV}$ is filled only upon inclusion of higher-order corrections. Similarly to the case of W^+W^- cuts, the behaviour of radiative effects is rather insensitive to the collider energy. Comparing NLO′+gg and full NNLO predictions, in spite of the fairly good agreement at the level of fiducial cross section, we observe that the genuine $\mathcal{O}(\alpha_{\rm S}^2)$ corrections lead to significant shape distortions at the 10% level.

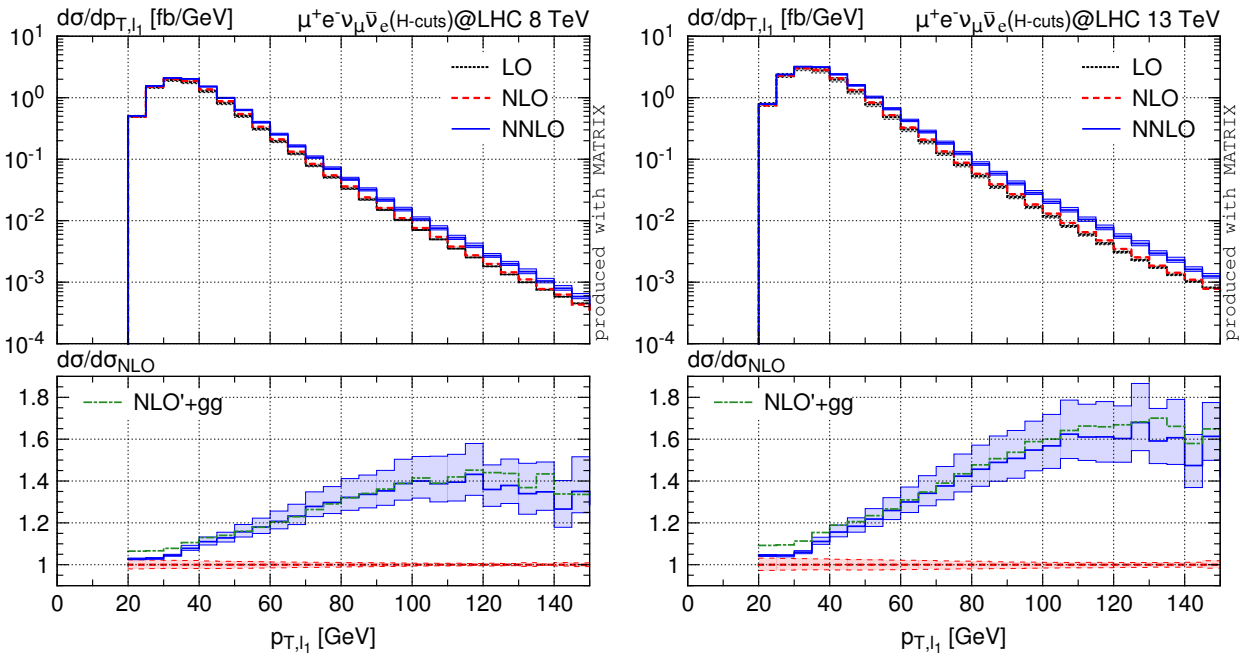

(a) (b)

Figure 20: Distribution in the p_T of the leading lepton. Higgs cuts are applied. Absolute predictions and relative corrections as in Figure 4.

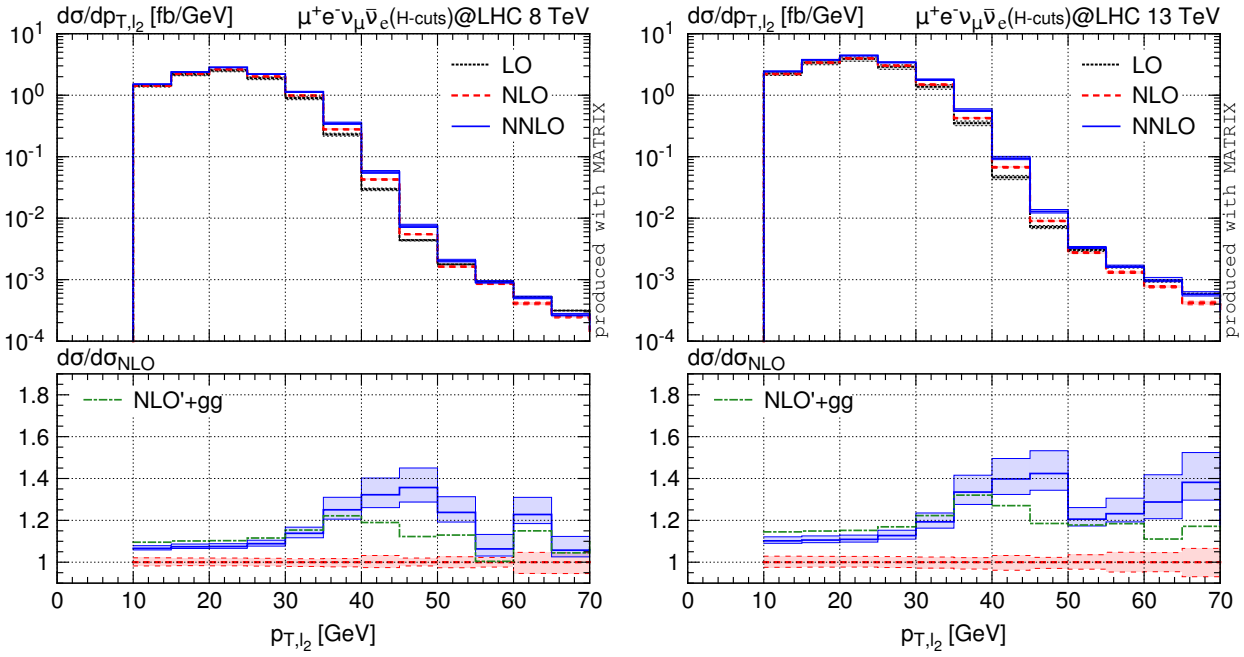

(a) (b)

Figure 21: Distribution in the p_T of the subleading lepton. Higgs cuts are applied. Absolute predictions and relative corrections as in Figure 4.

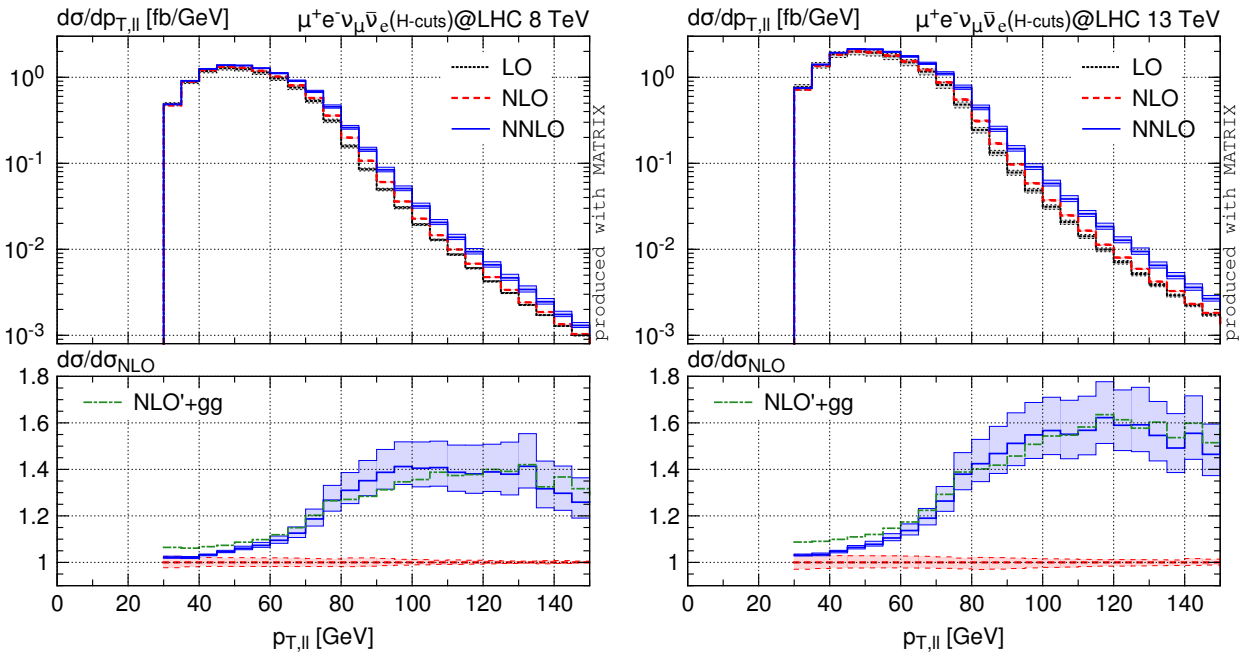

(a) (b)

Figure 22: Distribution in the p_T of the dilepton system. Higgs cuts are applied. Absolute predictions and relative corrections as in Figure 4.

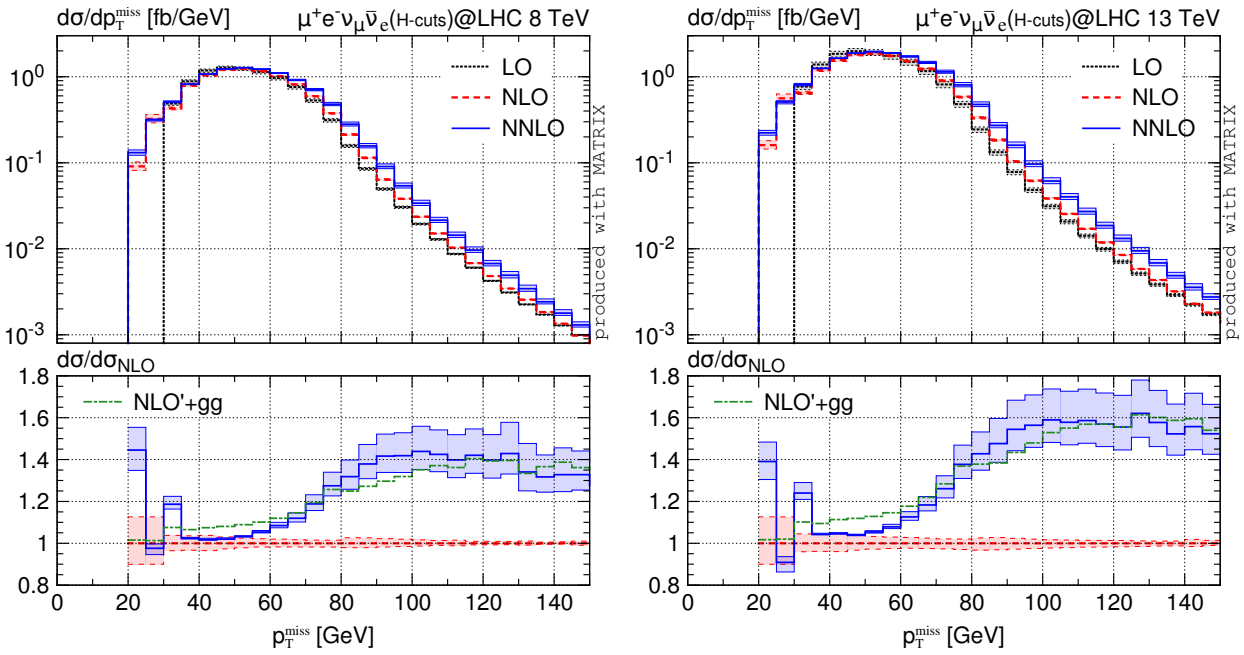

(a) (b)

Figure 23: Distribution in the missing transverse momentum. Higgs cuts are applied. Absolute predictions and relative corrections as in Figure 4.

4 Summary

We have presented the first fully differential calculation of the NNLO QCD corrections to W^+W^- production with decays at the LHC. Off-shell effects and spin correlations, as well as all possible topologies that lead to a final state with two charged leptons and two neutrinos are consistently taken into account in the complex-mass scheme. At higher orders in QCD perturbation theory, the inclusive W^+W^- cross section is plagued by a huge contamination from top-quark production processes, and the subtraction of top contributions is mandatory for a perturbatively stable definition of the W^+W^- rate. In our calculation, any top contamination is avoided by excluding partonic channels with final-state bottom quarks in the 4FS, where the bottom-quark mass renders such contributions separately finite. In order to quantify the sensitivity of the top-free W^+W^- cross section on the details of the top-subtraction prescription, our default predictions in the 4FS have been compared to an alternative calculation in the 5FS. In the latter case a numerical extrapolation in the narrow top-width limit is used to separate contributions that involve top resonances from genuine W^+W^- production and its interference with tW and $t\bar{t}$ production. The comparison of 4FS and 5FS predictions for inclusive and fiducial cross sections indicates that the dependence on the top-subtraction prescription is at the $1\% - 2\%$ level.

Numerical predictions at $\sqrt{s} = 8$ and 13 TeV have been discussed in detail for the different-flavour channel $pp \to \mu^+e^-\nu_\mu\bar{\nu}_e + X$. As compared to the case of on-shell W^+W^- production [46], the inclusion of leptonic decays leads to a reduction of the total cross section that corresponds to the effect of leptonic branching ratios plus an additional correction of about -2% due to off-shell effects. The influence of off-shell W-boson decays on the behaviour of (N)NLO QCD corrections is negligible. In fact, apart from minor differences due to the employed PDFs, we find that the relative impact of QCD corrections on the total cross sections is the same as for on-shell W^+W^- production [46]. At $\sqrt{s} = 8\,(13)$ TeV, ignoring the shift of $+2\%\,(+3\%)$ due to the difference between NNLO and NLO PDFs, the overall NNLO correction is as large as $+9\%\,(+11\%)$, while the loop-induced gluon–gluon contribution amounts to only $+3\%\,(+4\%)$; i.e., contrary to what was generally expected in the literature, the NNLO corrections are dominated by genuine NNLO contributions to the $q\bar{q}$ channel, and the loop-induced gg contribution plays only a subdominant role.

The complete calculation of NNLO QCD corrections allows us to provide a first realistic estimate of theoretical uncertainties through scale variations: As is well-known, uncertainties from missing higher-order contributions obtained through scale variations are completely unreliable at LO and still largely underestimated at NLO. This is due to the fact that the qg (as well as $\bar{q}g$) and gg (as well as $qq^{(\prime)}$, $\bar{q}\bar{q}^{(\prime)}$ and $q\bar{q}'$) partonic channels do not contribute at LO and NLO, respectively. In fact, NNLO is the first order at which all partonic channels contribute. Thus NNLO scale variations, which are at the level of $2\% - 3\%$ for the inclusive cross sections, can be regarded as a reasonable estimate of the theoretical uncertainty due to the truncation of the perturbative series. This is supported by the moderate impact of the recently computed NLO corrections to the loop-induced gg contribution [37].

Imposing a jet veto has a strong influence on the size of NNLO corrections and on the relative importance of NNLO contributions from the $q\bar{q}$ channel and the loop-induced gg channel. This was studied in detail for the case of standard fiducial cuts used in W^+W^- and $H \to W^+W^-$ analyses by the LHC experiments. As a result of the jet veto, such cuts significantly suppress all

(N)NLO contributions that involve QCD radiation, thereby enhancing the relative importance of the loop-induced gg channel at NNLO. More precisely, depending on the analysis and the collider energy, fiducial cuts lift the loop-induced gg contribution up to $6\% - 13\%$ with respect to NLO, whereas the genuine NNLO corrections to the $q\bar{q}$ channel are negative and range between -1% and -4%, while the NLO corrections vary between $+1\%$ and $+5\%$. The reduction of the impact of radiative corrections is accompanied by a reduction of scale uncertainties, which, for the NNLO fiducial cross sections, are at the $1\% - 2\%$ level. This is a typical side-effect of jet vetoes, and scale uncertainties are likely to underestimate unknown higher-order effects in this situation.

As a result of the different behaviour of radiative corrections to the inclusive and fiducial cross sections, their ratios, which determine the efficiencies of acceptance cuts, turn out to be quite sensitive to higher-order effects. More explicitly, the overall NNLO corrections to the cut efficiency are small and range between -3% and -1%. However, they arise from a positive shift between $+3\%$ and $+9\%$ due to the loop-induced gg channel, and a negative shift between -6% and -10% from genuine NNLO corrections to the $q\bar{q}$ channel. The NLO prediction supplemented by the loop-induced gg channel, i.e. the "best" prediction before the complete NNLO corrections were known, would thus lead to a significant overestimation of the efficiency, by up to about 10%. Similarly to the case of fiducial cross sections, the scale uncertainties of cut efficiencies are at the 1% level, and further studies are needed in order to estimate unknown higher-order effects in a fully realistic way. This, in particular, involves a more accurate modelling of the jet veto, which is left for future work.

Our analysis of differential distributions demonstrates that, in absence of fiducial cuts, genuine NNLO corrections to the $q\bar{q}$ channel can lead to significant modifications in the shapes of observables that are sensitive to QCD radiation, such as the transverse momentum of the leading W boson or of the W^+W^- system. On the other hand, in presence of fiducial cuts, NLO predictions supplemented with the loop-induced gg contribution yield a reasonably good description of the shape of differential observables, such as dilepton invariant masses and single-lepton transverse momenta. We find, however, that even for standard W^+W^- and Higgs selection cuts, which include a jet veto, genuine NNLO corrections tend to distort such distributions by up to about 10%. In phase-space regions that imply the presence of QCD radiation, loop-induced gg contributions cannot approximate the shapes of full NNLO corrections.

The predictions presented in this paper have been obtained with Matrix, a widely automated and flexible framework that supports NNLO calculations for all processes of the class $pp \to l^+l'^-\nu_l\bar{\nu}_{l'} + X$, including in particular also the channels with equal lepton flavours, $l = l'$. More generally, Matrix is able to address fully exclusive NNLO computations for all diboson production processes at hadron colliders.

Acknowledgements. We thank A. Denner, S. Dittmaier and L. Hofer for providing us with the one-loop tensor-integral library Collier well before publication, and we are grateful to P. Maierhöfer and J. Lindert for advice on technical aspects of OpenLoops. This research was supported in part by the Swiss National Science Foundation (SNF) under contracts 200020-141360, 200021-156585, CRSII2-141847, BSCGI0-157722 and PP00P2-153027, and by the Kavli Institute for Theoretical Physics through the National Science Foundation's Grant No. NSF PHY11-25915.

References

[1] **CDF** Collaboration, T. Aaltonen et al., *Measurement of the W^+W^- Production Cross Section and Search for Anomalous $WW\gamma$ and WWZ Couplings in $p\bar{p}$ Collisions at $\sqrt{s} = 1.96$ TeV*, Phys. Rev. Lett. **104** (2010) 201801, [arXiv:0912.4500].

[2] **D0** Collaboration, V. M. Abazov et al., *Measurements of WW and WZ production in W + jets final states in $p\bar{p}$ collisions*, Phys. Rev. Lett. **108** (2012) 181803, [arXiv:1112.0536].

[3] **ATLAS** Collaboration, G. Aad et al., *Measurement of W^+W^- production in pp collisions at $\sqrt{s}$=7 TeV with the ATLAS detector and limits on anomalous WWZ and $WW\gamma$ couplings*, Phys.Rev. **D87** (2013), no. 11 112001, [arXiv:1210.2979].

[4] **CMS** Collaboration, S. Chatrchyan et al., *Measurement of the W^+W^- Cross section in pp Collisions at $\sqrt{s} = 7$ TeV and Limits on Anomalous $WW\gamma$ and WWZ couplings*, Eur. Phys. J. **C73** (2013), no. 10 2610, [arXiv:1306.1126].

[5] **ATLAS** Collaboration, *Measurement of the W^+W^- production cross section in proton-proton collisions at $\sqrt{s} = 8$ TeV with the ATLAS detector*, ATLAS-CONF-2014-033.

[6] **ATLAS** Collaboration, G. Aad et al., *Measurement of total and differential W^+W^- production cross sections in proton-proton collisions at $\sqrt{s} = 8$ TeV with the ATLAS detector and limits on anomalous triple-gauge-boson couplings*, arXiv:1603.01702.

[7] **CMS** Collaboration, S. Chatrchyan et al., *Measurement of W+W- and ZZ production cross sections in pp collisions at sqrt(s) = 8 TeV*, Phys. Lett. **B721** (2013) 190–211, [arXiv:1301.4698].

[8] **CMS** Collaboration, V. Khachatryan et al., *Measurement of the W^+W^- cross section in pp collisions at $\sqrt{s} = 8$ TeV and limits on anomalous gauge couplings*, arXiv:1507.03268.

[9] **ATLAS, CDF, CMS, D0** Collaboration, J. Wang, *Diboson Production at LHC and Tevatron*, Int. J. Mod. Phys. Conf. Ser. **31** (2014) 1460279, [arXiv:1403.1415].

[10] D. E. Morrissey, T. Plehn, and T. M. Tait, *Physics searches at the LHC*, Phys.Rept. **515** (2012) 1–113, [arXiv:0912.3259].

[11] **ATLAS** Collaboration, G. Aad et al., *Observation of a new particle in the search for the Standard Model Higgs boson with the ATLAS detector at the LHC*, Phys. Lett. **B716** (2012) 1–29, [arXiv:1207.7214].

[12] **ATLAS** Collaboration, G. Aad et al., *Observation and measurement of Higgs boson decays to WW^* with the ATLAS detector*, Phys. Rev. **D92** (2015), no. 1 012006, [arXiv:1412.2641].

[13] **ATLAS** Collaboration, G. Aad et al., *Measurement of fiducial differential cross sections of gluon-fusion production of Higgs bosons decaying to $WW^* \to e\nu\mu\nu$ with the ATLAS detector at $\sqrt{s} = 8$ TeV*, arXiv:1604.02997.

[14] **CMS** Collaboration, S. Chatrchyan et al., *Observation of a new boson at a mass of 125 GeV with the CMS experiment at the LHC*, Phys. Lett. **B716** (2012) 30–61, [arXiv:1207.7235].

[15] **CMS** Collaboration, S. Chatrchyan et al., *Observation of a new boson with mass near 125 GeV in pp collisions at $\sqrt{s}$ = 7 and 8 TeV*, JHEP **06** (2013) 081, [arXiv:1303.4571].

[16] **CMS** Collaboration, S. Chatrchyan et al., *Measurement of Higgs boson production and properties in the WW decay channel with leptonic final states*, JHEP **01** (2014) 096, [arXiv:1312.1129].

[17] N. Kauer and G. Passarino, *Inadequacy of zero-width approximation for a light Higgs boson signal*, JHEP **1208** (2012) 116, [arXiv:1206.4803].

[18] F. Caola and K. Melnikov, *Constraining the Higgs boson width with ZZ production at the LHC*, Phys.Rev. **D88** (2013) 054024, [arXiv:1307.4935].

[19] J. M. Campbell, R. K. Ellis, and C. Williams, *Bounding the Higgs width at the LHC: Complementary results from $H \to WW$*, Phys.Rev. **D89** (2014), no. 5 053011, [arXiv:1312.1628].

[20] J. Ohnemus, *An Order α_s calculation of hadronic W^-W^+ production*, Phys.Rev. **D44** (1991) 1403–1414.

[21] S. Frixione, *A Next-to-leading order calculation of the cross-section for the production of W^+W^- pairs in hadronic collisions*, Nucl.Phys. **B410** (1993) 280–324.

[22] J. M. Campbell and R. K. Ellis, *An Update on vector boson pair production at hadron colliders*, Phys.Rev. **D60** (1999) 113006, [hep-ph/9905386].

[23] L. J. Dixon, Z. Kunszt, and A. Signer, *Vector boson pair production in hadronic collisions at order α_s : Lepton correlations and anomalous couplings*, Phys.Rev. **D60** (1999) 114037, [hep-ph/9907305].

[24] L. J. Dixon, Z. Kunszt, and A. Signer, *Helicity amplitudes for $O(\alpha_s)$ production of W^+W^-, $W^\pm Z$, ZZ, $W^\pm\gamma$, or $Z\gamma$ pairs at hadron colliders*, Nucl.Phys. **B531** (1998) 3–23, [hep-ph/9803250].

[25] J. M. Campbell, R. K. Ellis, and C. Williams, *Vector boson pair production at the LHC*, JHEP **1107** (2011) 018, [arXiv:1105.0020].

[26] A. Bierweiler, T. Kasprzik, J. H. Kühn, and S. Uccirati, *Electroweak corrections to W-boson pair production at the LHC*, JHEP **1211** (2012) 093, [arXiv:1208.3147].

[27] J. Baglio, L. D. Ninh, and M. M. Weber, *Massive gauge boson pair production at the LHC: a next-to-leading order story*, Phys.Rev. **D88** (2013) 113005, [arXiv:1307.4331].

[28] M. Billoni, S. Dittmaier, B. Jäger, and C. Speckner, *Next-to-leading order electroweak corrections to $pp \to W^+W^- \to 4$ leptons at the LHC in double-pole approximation*, JHEP **1312** (2013) 043, [arXiv:1310.1564].

[29] D. A. Dicus, C. Kao, and W. Repko, *Gluon Production of Gauge Bosons*, Phys.Rev. **D36** (1987) 1570.

[30] E. N. Glover and J. van der Bij, *Vector boson pair production via gluon fusion*, Phys.Lett. **B219** (1989) 488.

[31] T. Binoth, M. Ciccolini, N. Kauer, and M. Krämer, *Gluon-induced WW background to Higgs boson searches at the LHC*, JHEP **0503** (2005) 065, [hep-ph/0503094].

[32] T. Binoth, M. Ciccolini, N. Kauer, and M. Krämer, *Gluon-induced W-boson pair production at the LHC*, JHEP **0612** (2006) 046, [hep-ph/0611170].

[33] T. Melia, P. Nason, R. Röntsch, and G. Zanderighi, *W+W-, WZ and ZZ production in the POWHEG BOX*, JHEP **1111** (2011) 078, [arXiv:1107.5051].

[34] T. Melia, K. Melnikov, R. Röntsch, M. Schulze, and G. Zanderighi, *Gluon fusion contribution to W+W- + jet production*, JHEP **1208** (2012) 115, [arXiv:1205.6987].

[35] F. Caola, J. M. Henn, K. Melnikov, A. V. Smirnov, and V. A. Smirnov, *Two-loop helicity amplitudes for the production of two off-shell electroweak bosons in gluon fusion*, JHEP **1506** (2015) 129, [arXiv:1503.08759].

[36] A. von Manteuffel and L. Tancredi, *The two-loop helicity amplitudes for $gg \to V_1V_2 \to 4$ leptons*, JHEP **1506** (2015) 197, [arXiv:1503.08835].

[37] F. Caola, K. Melnikov, R. Röntsch, and L. Tancredi, *QCD Corrections to W^+W^- Production through Gluon Fusion*, arXiv:1511.08617.

[38] S. Dittmaier, S. Kallweit, and P. Uwer, *NLO QCD corrections to WW+jet production at hadron colliders*, Phys.Rev.Lett. **100** (2008) 062003, [arXiv:0710.1577].

[39] J. M. Campbell, R. K. Ellis, and G. Zanderighi, *Next-to-leading order predictions for $WW + 1$ jet distributions at the LHC*, JHEP **0712** (2007) 056, [arXiv:0710.1832].

[40] S. Dittmaier, S. Kallweit, and P. Uwer, *NLO QCD corrections to $pp/p\bar{p} \to WW$+jet+X including leptonic W-boson decays*, Nucl.Phys. **B826** (2010) 18–70, [arXiv:0908.4124].

[41] J. M. Campbell, D. J. Miller, and T. Robens, *Next-to-Leading Order Predictions for WW+Jet Production*, Phys. Rev. **D92** (2015), no. 1 014033, [arXiv:1506.04801].

[42] T. Melia, K. Melnikov, R. Röntsch, and G. Zanderighi, *NLO QCD corrections for W^+W^- pair production in association with two jets at hadron colliders*, Phys.Rev. **D83** (2011) 114043, [arXiv:1104.2327].

[43] N. Greiner, G. Heinrich, P. Mastrolia, G. Ossola, T. Reiter, and F. Tramontano, *NLO QCD corrections to the production of W^+W^- plus two jets at the LHC*, Phys.Lett. **B713** (2012) 277–283, [arXiv:1202.6004].

[44] F. Campanario, M. Rauch, and S. Sapeta, *W^+W^- production at high transverse momenta beyond NLO*, Nucl. Phys. **B879** (2014) 65–79, [arXiv:1309.7293].

[45] F. Cascioli, S. Höche, F. Krauss, P. Maierhöfer, S. Pozzorini, and F. Siegert, *Precise Higgs-background predictions: merging NLO QCD and squared quark-loop corrections to four-lepton + 0,1 jet production*, JHEP **1401** (2014) 046, [arXiv:1309.0500].

[46] T. Gehrmann, M. Grazzini, S. Kallweit, P. Maierhöfer, A. von Manteuffel, S. Pozzorini, D. Rathlev, and L. Tancredi, *W^+W^- Production at Hadron Colliders in Next to Next to Leading Order QCD*, Phys.Rev.Lett. **113** (2014) 212001, [arXiv:1408.5243].

[47] F. Caola, J. M. Henn, K. Melnikov, A. V. Smirnov, and V. A. Smirnov, *Two-loop helicity amplitudes for the production of two off-shell electroweak bosons in quark-antiquark collisions*, JHEP **1411** (2014) 041, [arXiv:1408.6409].

[48] T. Gehrmann, A. von Manteuffel, and L. Tancredi, *The two-loop helicity amplitudes for $q\bar{q}' \to V_1 V_2 \to 4$ leptons*, arXiv:1503.04812.

[49] P. Nason and G. Zanderighi, *W^+W^- , WZ and ZZ production in the POWHEG-BOX-V2*, Eur. Phys. J. **C74** (2014), no. 1 2702, [arXiv:1311.1365].

[50] P. F. Monni and G. Zanderighi, *On the excess in the inclusive $W^+W^- \to l^+l^-\nu\bar{\nu}$ cross section*, JHEP **1505** (2015) 013, [arXiv:1410.4745].

[51] P. Jaiswal and T. Okui, *Explanation of the WW excess at the LHC by jet-veto resummation*, Phys.Rev. **D90** (2014), no. 7 073009, [arXiv:1407.4537].

[52] T. Becher, R. Frederix, M. Neubert, and L. Rothen, *Automated NNLL + NLO resummation for jet-veto cross sections*, Eur.Phys.J. **C75** (2015), no. 4 154, [arXiv:1412.8408].

[53] M. Grazzini, S. Kallweit, D. Rathlev, and M. Wiesemann, *Transverse-momentum resummation for vector-boson pair production at NNLL+NNLO*, JHEP **08** (2015) 154, [arXiv:1507.02565].

[54] A. Denner, S. Dittmaier, M. Roth, and L. H. Wieders, *Electroweak corrections to charged-current $e^+e^- \to 4$ fermion processes: Technical details and further results*, Nucl. Phys. **B724** (2005) 247–294, [hep-ph/0505042]. [Erratum: Nucl. Phys.B854,504(2012)].

[55] MATRIX is the abbreviation of "MUNICH Automates qT subtraction and Resummation to Integrate X-sections", by M. Grazzini, S. Kallweit, D. Rathlev, and M. Wiesemann. In preparation.

[56] MUNICH is the abbreviation of "MUlti-chaNnel Integrator at Swiss (CH) precision"—an automated parton level NLO generator by S. Kallweit. In preparation.

[57] F. Cascioli, P. Maierhöfer, and S. Pozzorini, *Scattering Amplitudes with Open Loops*, Phys.Rev.Lett. **108** (2012) 111601, [arXiv:1111.5206].

[58] The OPENLOOPS one-loop generator, by F. Cascioli, J. Lindert, P. Maierhöfer, and S. Pozzorini, is publicly available at http://openloops.hepforge.org.

[59] S. Catani and M. Grazzini, *An NNLO subtraction formalism in hadron collisions and its application to Higgs boson production at the LHC*, Phys.Rev.Lett. **98** (2007) 222002, [hep-ph/0703012].

[60] G. Bozzi, S. Catani, D. de Florian, and M. Grazzini, *Transverse-momentum resummation and the spectrum of the Higgs boson at the LHC*, Nucl.Phys. **B737** (2006) 73–120, [hep-ph/0508068].

[61] T. Gehrmann and L. Tancredi, *Two-loop QCD helicity amplitudes for $q\bar{q} \to W^{\pm}\gamma$ and $q\bar{q} \to Z^0\gamma$*, JHEP **02** (2012) 004, [arXiv:1112.1531].

[62] M. Grazzini, S. Kallweit, D. Rathlev, and A. Torre, *$Z\gamma$ production at hadron colliders in NNLO QCD*, Phys.Lett. **B731** (2014) 204–207, [arXiv:1309.7000].

[63] M. Grazzini, S. Kallweit, and D. Rathlev, *$W\gamma$ and $Z\gamma$ production at the LHC in NNLO QCD*, JHEP **07** (2015) 085, [arXiv:1504.01330].

[64] F. Cascioli, T. Gehrmann, M. Grazzini, S. Kallweit, P. Maierhöfer, A. von Manteuffel, S. Pozzorini, D. Rathlev, L. Tancredi, and E. Weihs, *ZZ production at hadron colliders in NNLO QCD*, Phys.Lett. **B735** (2014) 311–313, [arXiv:1405.2219].

[65] M. Grazzini, S. Kallweit, and D. Rathlev, *ZZ production at the LHC: fiducial cross sections and distributions in NNLO QCD*, Phys. Lett. **B750** (2015) 407–410, [arXiv:1507.06257].

[66] M. Grazzini, S. Kallweit, D. Rathlev, and M. Wiesemann, *$W^{\pm}Z$ production at hadron colliders in NNLO QCD*, arXiv:1604.08576.

[67] A. Denner, S. Dittmaier, and L. Hofer, *COLLIER - A fortran-library for one-loop integrals*, PoS **LL2014** (2014) 071, [arXiv:1407.0087].

[68] A. Denner, S. Dittmaier, and L. Hofer, *Collier: a fortran-based Complex One-Loop LIbrary in Extended Regularizations*, arXiv:1604.06792.

[69] Collier - A Complex One-Loop LIbrary with Extended Regularizations, by A. Denner, S. Dittmaier, and L. Hofer, is publicly available at http://collier.hepforge.org.

[70] A. Denner and S. Dittmaier, *Reduction of one loop tensor five point integrals*, Nucl.Phys. **B658** (2003) 175–202, [hep-ph/0212259].

[71] A. Denner and S. Dittmaier, *Reduction schemes for one-loop tensor integrals*, Nucl.Phys. **B734** (2006) 62–115, [hep-ph/0509141].

[72] A. Denner and S. Dittmaier, *Scalar one-loop 4-point integrals*, Nucl.Phys. **B844** (2011) 199–242, [arXiv:1005.2076].

[73] The VVamp project, by T. Gehrmann, A. von Manteuffel, and L. Tancredi, is publicly available at http://vvamp.hepforge.org.

[74] J. Vollinga and S. Weinzierl, *Numerical evaluation of multiple polylogarithms*, Comput. Phys. Commun. **167** (2005) 177, [hep-ph/0410259].

[75] C. W. Bauer, A. Frink, and R. Kreckel, *Introduction to the GiNaC framework for symbolic computation within the C++ programming language*, J. Symb. Comput. **33** (2000) 1, [cs/0004015].

[76] D. A. Kosower, *Antenna factorization of gauge theory amplitudes*, Phys. Rev. **D57** (1998) 5410–5416, [hep-ph/9710213].

[77] A. Gehrmann-De Ridder, T. Gehrmann, and E. W. N. Glover, *Antenna subtraction at NNLO*, JHEP **09** (2005) 056, [hep-ph/0505111].

[78] A. Daleo, T. Gehrmann, and D. Maitre, *Antenna subtraction with hadronic initial states*, JHEP **04** (2007) 016, [hep-ph/0612257].

[79] J. Currie, E. W. N. Glover, and S. Wells, *Infrared Structure at NNLO Using Antenna Subtraction*, JHEP **04** (2013) 066, [arXiv:1301.4693].

[80] G. Somogyi, Z. Trocsanyi, and V. Del Duca, *Matching of singly- and doubly-unresolved limits of tree-level QCD squared matrix elements*, JHEP **06** (2005) 024, [hep-ph/0502226].

[81] V. Del Duca, C. Duhr, G. Somogyi, F. Tramontano, and Z. Trocsanyi, *Higgs boson decay into b-quarks at NNLO accuracy*, JHEP **04** (2015) 036, [arXiv:1501.07226].

[82] V. Del Duca, C. Duhr, A. Kardos, G. Somogyi, and Z. Trócsányi, *Three-jet production in electron-positron collisions using the CoLoRFulNNLO method*, arXiv:1603.08927.

[83] M. Czakon, *A novel subtraction scheme for double-real radiation at NNLO*, Phys. Lett. **B693** (2010) 259–268, [arXiv:1005.0274].

[84] M. Czakon, *Double-real radiation in hadronic top quark pair production as a proof of a certain concept*, Nucl. Phys. **B849** (2011) 250–295, [arXiv:1101.0642].

[85] M. Czakon and D. Heymes, *Four-dimensional formulation of the sector-improved residue subtraction scheme*, Nucl. Phys. **B890** (2014) 152–227, [arXiv:1408.2500].

[86] S. Frixione, Z. Kunszt, and A. Signer, *Three jet cross-sections to next-to-leading order*, Nucl. Phys. **B467** (1996) 399–442, [hep-ph/9512328].

[87] S. Frixione, *A General approach to jet cross-sections in QCD*, Nucl. Phys. **B507** (1997) 295–314, [hep-ph/9706545].

[88] S. Catani and M. Seymour, *The Dipole formalism for the calculation of QCD jet cross-sections at next-to-leading order*, Phys.Lett. **B378** (1996) 287–301, [hep-ph/9602277].

[89] S. Catani and M. Seymour, *A General algorithm for calculating jet cross-sections in NLO QCD*, Nucl.Phys. **B485** (1997) 291–419, [hep-ph/9605323].

[90] C. Anastasiou, K. Melnikov, and F. Petriello, *A new method for real radiation at NNLO*, Phys. Rev. **D69** (2004) 076010, [hep-ph/0311311].

[91] T. Binoth and G. Heinrich, *An automatized algorithm to compute infrared divergent multiloop integrals*, Nucl. Phys. **B585** (2000) 741–759, [hep-ph/0004013].

[92] R. Boughezal, C. Focke, X. Liu, and F. Petriello, *W-boson production in association with a jet at next-to-next-to-leading order in perturbative QCD*, Phys. Rev. Lett. **115** (2015), no. 6 062002, [arXiv:1504.02131].

[93] R. Boughezal, X. Liu, and F. Petriello, *N-jettiness soft function at next-to-next-to-leading order*, Phys. Rev. **D91** (2015), no. 9 094035, [arXiv:1504.02540].

[94] J. Gaunt, M. Stahlhofen, F. J. Tackmann, and J. R. Walsh, *N-jettiness Subtractions for NNLO QCD Calculations*, JHEP **09** (2015) 058, [arXiv:1505.04794].

[95] M. Cacciari, F. A. Dreyer, A. Karlberg, G. P. Salam, and G. Zanderighi, *Fully Differential Vector-Boson-Fusion Higgs Production at Next-to-Next-to-Leading Order*, Phys. Rev. Lett. **115** (2015), no. 8 082002, [arXiv:1506.02660].

[96] R. Bonciani, S. Catani, M. Grazzini, H. Sargsyan, and A. Torre, *The q_T subtraction method for top quark production at hadron colliders*, Eur. Phys. J. **C75** (2015), no. 12 581, [arXiv:1508.03585].

[97] S. Catani, L. Cieri, G. Ferrera, D. de Florian, and M. Grazzini, *Vector boson production at hadron colliders: a fully exclusive QCD calculation at NNLO*, Phys.Rev.Lett. **103** (2009) 082001, [arXiv:0903.2120].

[98] G. Ferrera, M. Grazzini, and F. Tramontano, *Associated WH production at hadron colliders: a fully exclusive QCD calculation at NNLO*, Phys.Rev.Lett. **107** (2011) 152003, [arXiv:1107.1164].

[99] S. Catani, L. Cieri, D. de Florian, G. Ferrera, and M. Grazzini, *Diphoton production at hadron colliders: a fully-differential QCD calculation at NNLO*, Phys.Rev.Lett. **108** (2012) 072001, [arXiv:1110.2375].

[100] G. Ferrera, M. Grazzini, and F. Tramontano, *Associated ZH production at hadron colliders: the fully differential NNLO QCD calculation*, Phys.Lett. **B740** (2015) 51–55, [arXiv:1407.4747].

[101] D. de Florian and M. Grazzini, *The Structure of large logarithmic corrections at small transverse momentum in hadronic collisions*, Nucl.Phys. **B616** (2001) 247–285, [hep-ph/0108273].

[102] S. Catani and M. Grazzini, *Higgs Boson Production at Hadron Colliders: Hard-Collinear Coefficients at the NNLO*, Eur.Phys.J. **C72** (2012) 2013, [arXiv:1106.4652].

[103] S. Catani, L. Cieri, D. de Florian, G. Ferrera, and M. Grazzini, *Vector boson production at hadron colliders: hard-collinear coefficients at the NNLO*, Eur.Phys.J. **C72** (2012) 2195, [arXiv:1209.0158].

[104] S. Catani, L. Cieri, D. de Florian, G. Ferrera, and M. Grazzini, *Universality of transverse-momentum resummation and hard factors at the NNLO*, Nucl.Phys. **B881** (2014) 414–443, [arXiv:1311.1654].

[105] T. Gehrmann, T. Lübbert, and L. L. Yang, *Transverse parton distribution functions at next-to-next-to-leading order: the quark-to-quark case*, Phys.Rev.Lett. **109** (2012) 242003, [arXiv:1209.0682].

[106] T. Gehrmann, T. Lübbert, and L. L. Yang, *Calculation of the transverse parton distribution functions at next-to-next-to-leading order*, JHEP **1406** (2014) 155, [arXiv:1403.6451].

[107] M. Wiesemann, *Transverse-momentum resummation of colorless final states at the NNLL+NNLO*, 2016. arXiv:1602.03401.

[108] **Particle Data Group** Collaboration, K. Olive et al., *Review of Particle Physics*, Chin.Phys. **C38** (2014) 090001.

[109] **NNPDF** Collaboration, R. D. Ball et al., *Parton distributions for the LHC Run II*, JHEP **1504** (2015) 040, [arXiv:1410.8849].

[110] M. Cacciari, G. P. Salam, and G. Soyez, *The Anti-k(t) jet clustering algorithm*, JHEP **0804** (2008) 063, [arXiv:0802.1189].

[111] S. Catani, D. de Florian, and M. Grazzini, *Direct Higgs production and jet veto at the Tevatron and the LHC in NNLO QCD*, JHEP **01** (2002) 015, [hep-ph/0111164].

[112] A. Banfi, P. F. Monni, G. P. Salam, and G. Zanderighi, *Higgs and Z-boson production with a jet veto*, Phys. Rev. Lett. **109** (2012) 202001, [arXiv:1206.4998].

[113] T. Becher and M. Neubert, *Factorization and NNLL Resummation for Higgs Production with a Jet Veto*, JHEP **07** (2012) 108, [arXiv:1205.3806].

[114] I. W. Stewart, F. J. Tackmann, J. R. Walsh, and S. Zuberi, *Jet p_T resummation in Higgs production at $NNLL' + NNLO$*, Phys. Rev. **D89** (2014), no. 5 054001, [arXiv:1307.1808].

[115] S. Catani and B. R. Webber, *Infrared safe but infinite: Soft gluon divergences inside the physical region*, JHEP **10** (1997) 005, [hep-ph/9710333].